

# Spatio-temporal dynamics of large-scale electrophysiological networks during cognitive action control in healthy controls and Parkinson's disease patients

Joan Duprez, Judie Tabbal, Mahmoud Hassan, Julien Modolo, Aya Kabbara, Ahmad Mheich, Sophie Drapier, Marc Verin, Paul Sauleau, Fabrice Wendling, et al.

▶ **To cite this version:**

Joan Duprez, Judie Tabbal, Mahmoud Hassan, Julien Modolo, Aya Kabbara, et al.. Spatio-temporal dynamics of large-scale electrophysiological networks during cognitive action control in healthy controls and Parkinson's disease patients. NeuroImage, 2022, 258, pp.119331. 10.1016/j.neuroimage.2022.119331 . hal-03716156

**HAL Id: hal-03716156**
**https://hal.science/hal-03716156**

Submitted on 23 Jan 2023

**HAL** is a multi-disciplinary open access archive for the deposit and dissemination of scientific research documents, whether they are published or not. The documents may come from teaching and research institutions in France or abroad, or from public or private research centers.

L'archive ouverte pluridisciplinaire **HAL**, est destinée au dépôt et à la diffusion de documents scientifiques de niveau recherche, publiés ou non, émanant des établissements d'enseignement et de recherche français ou étrangers, des laboratoires publics ou privés.



Distributed under a Creative Commons Attribution - NonCommercial - NoDerivatives 4.0 International License

NeuroImage 258 (2022) 119331

Contents lists available at ScienceDirect

NeuroImage

journal homepage: www.elsevier.com/locate/neuroimage

# Spatio-temporal dynamics of large-scale electrophysiological networks during cognitive action control in healthy controls and Parkinson's disease patients

Joan Duprez[a,#,*], Judie Tabbal[a,b,#], Mahmoud Hassan[c,d], Julien Modolo[a], Aya Kabbara[c], Ahmad Mheich[e], Sophie Drapier[f,g], Marc Vérin[g,h], Paul Sauleau[h,i], Fabrice Wendling[a], Pascal Benquet[a], Jean-François Houvenaghel[g,h]

[a] Univ Rennes, LTSI - U1099, F-35000 Rennes, France
[b] Azm Center for Research in Biotechnology and Its Applications, EDST, Lebanese University, Beirut, Lebanon
[c] MINDig, F-35000 Rennes, France
[d] School of Engineering, Reykjavik University, Iceland
[e] CHUV-Centre Hospitalier Universitaire Vaudois, Service des Troubles du Spectre de l'Autisme et apparentés, Lausanne University Hospital, Les Allières – Av. Beaumont 23, 1011, Lausanne, Switzerland
[f] CIC INSERM 1414, Rennes, France
[g] Neurology Department, Pontchaillou Hospital, Rennes University Hospital, France
[h] Behavioral and Basal Ganglia' Research Unit, University of Rennes 1-Rennes University Hospital, France
[i] Neurophysiology Department, Rennes University Hospital, France

ARTICLE INFO

*Keywords:*
Functional connectivity
Networks
Dynamics
High density EEG
Cognitive control
Simon task
Parkinson's disease

ABSTRACT

Among the cognitive symptoms that are associated with Parkinson's disease (PD), alterations in cognitive action control (CAC) are commonly reported in patients. CAC enables the suppression of an automatic action, in favor of a goal-directed one. The implementation of CAC is time-resolved and arguably associated with dynamic changes in functional brain networks. However, the electrophysiological functional networks involved, their dynamic changes, and how these changes are affected by PD, still remain unknown. In this study, to address this gap of knowledge, 10 PD patients and 10 healthy controls (HC) underwent a Simon task while high-density electroencephalography (HD-EEG) was recorded. Source-level dynamic connectivity matrices were estimated using the phase-locking value in the beta (12-25 Hz) and gamma (30-45 Hz) frequency bands. Temporal independent component analyses were used as a dimension reduction tool to isolate the task-related brain network states. Typical microstate metrics were quantified to investigate the presence of these states at the subject-level. Our results first confirmed that PD patients experienced difficulties in inhibiting automatic responses during the task. At the group-level, we found three functional network states in the beta band that involved fronto-temporal, temporo-cingulate and fronto-frontal connections with typical CAC-related prefrontal and cingulate nodes (e.g., inferior frontal cortex). The presence of these networks did not differ between PD patients and HC when analyzing microstates metrics, and no robust correlations with behavior were found. In the gamma band, five networks were found, including one fronto-temporal network that was identical to the one found in the beta band. These networks also included CAC-related nodes previously identified in different neuroimaging modalities. Similarly to the beta networks, no subject-level differences were found between PD patients and HC. Interestingly, in both

*Abbreviations:* CAC, Cognitive action control; dBNS, Dynamic brain network state; dFC, Dynamic functional connectivity; DIFFIT, Difference in data fitting; DLPFC, Dorso-lateral prefrontal cortex; EEG, Electroencephalography; FC, Functional connectivity; fMRI, Functional magnetic resonance imaging; HC, Healthy controls; HD-EEG, High-density EEG; ICA, Independent component analysis; IFC, Inferior frontal cortex; MEG, Magnetoencephalography; PD, Parkinson's disease; PLV, Phase locking value; pre-SMA, Pre-supplementary motor area; ROIS, Regions of interest; RT, Reaction time; tICA, Temporal ICA.

* Corresponding author:
*E-mail address:* joan.duprez@univ-rennes1.fr (J. Duprez).
# Equal contribution of authors.

https://doi.org/10.1016/j.neuroimage.2022.119331.
Received 13 December 2021; Received in revised form 16 May 2022; Accepted 23 May 2022
Available online 1 June 2022.
1053-8119/© 2022 The Author(s). Published by Elsevier Inc. This is an open access article under the CC BY-NC-ND license (http://creativecommons.org/licenses/by-nc-nd/4.0/)

frequency bands, the dominant network at the subject-level was never the one that was the most durably modulated by the task. Altogether, this study identified the dynamic functional brain networks observed during CAC, but did not highlight PD-related changes in these networks that might explain behavioral changes. Although other new methods might be needed to investigate the presence of task-related networks at the subject-level, this study still highlights that task-based dynamic functional connectivity is a promising approach in understanding the cognitive dysfunctions observed in PD and beyond.

## 1. Introduction

Parkinson's disease (PD) is associated with a broad spectrum of symptoms. Although it is mostly known for its deleterious effects on motor function, such as bradykinesia, rigidity and resting tremor (Hayes, 2019), cognitive impairments associated with PD also have a significant impact on quality of life (Lawson et al., 2016). One of the major cognitive difficulties found in PD patients is the impairment in efficient and fast adaptation to environmental changes. More specifically, PD patients typically show alterations in cognitive action control (CAC), a sub-process of cognitive control that enables the suppression of automatic responses in favor of goal-directed voluntary actions. CAC is usually measured using conflict tasks such as the Simon task (Simon and Rudell, 1967) in which participants have to respond according to a stimulus's color while ignoring its location. Incongruent situations in these tasks (when color and location lead to conflicting responses) result in an increase in reaction time (RT) and a decrease in accuracy, which is commonly termed the congruence effect. Dual route models (Hommel and Wiers, 2017) interpret this as the result of the competition between an automatic and fast route for response activation, and a controlled, slower one. The activation-suppression model (Ridderinkhof, 2002) enriched this view by adding a dynamic aspect stating that fast responses in incongruent trials are more error-prone (impulsive action selection), and that slower responses are associated with stronger inhibition because inhibitory processes had time to build-up. To date, numerous studies focused not only on the average congruence effect, but also on fast errors, to investigate impulsive action selection, and on the size of the congruence effect for the slowest responses, that reflects selective inhibition (see (van den Wildenberg et al., 2010)).

PD patients consistently show alterations regarding CAC compared to healthy controls (HC). However the nature of the impairment is somewhat inconsistent between studies. Indeed, alteration of CAC in PD was found through an increase in the congruence effect in PD patients on RT or accuracy, while others found decreased selective inhibition or an increase in impulsive fast errors but with no effect in average congruence effect(Cagigas et al., 2007; Duprez et al., 2017; Falkenstein et al., 2006; Wylie et al., 2010, 2005).

Importantly, even at the prodromal stages of PD, accumulation of $\alpha$-Synuclein results in synaptic and axonal dysfunctions (Bridi and Hirth, 2018). This could explain the presence of cognitive impairment that is sometimes already present at the time of diagnosis. Indeed, integrity and efficiency of synaptic communication is arguably important for processes requiring fast decision making such as CAC. Several studies have investigated the correlations between brain activity on the one hand, and cognitive changes on the other hand, using a variety of neuroimaging modalities (fMRI, PET, (M)/EEG). For instance, it is now undisputed that conflict resolution is associated with activity in the dorso-lateral prefrontal cortex (DLPFC), the inferior frontal cortex (IFC), the pre-supplementary motor area (pre-SMA), the anterior cingulate cortex, and the subthalamic nucleus (Ridderinkhof et al., 2011). In addition to this localizationist approach, studying the interaction between brain regions would help in specifying how neurodegenerative diseases such as PD alter cognitive functions. Indeed, a large body of evidence now shows that cognitive functioning emerges from the communication of distant brain regions (Bassett and Sporns, 2017) and that alterations in these brain networks have been associated with neurological disorders (Fornito et al., 2015). Brain networks can be studied, among available techniques, *via* the estimation of functional connectivity (FC) between brain areas, as estimated from electrophysiological ((M)EEG) or metabolic (MRI, PET) signals. FC is not in itself a direct measure of communication between brain areas, but rather reflects statistical dependencies of brain activity between different regions. (M)EEG FC is particularly interesting since it is usually inferred through the phase synchronization of neural oscillations, a mechanism that has been proposed to facilitate communication between neuronal assemblies (Fries, 2015). A growing body of literature has shown that neural oscillations in different frequency bands are associated with cognition. For instance, beta activity has been suggested to implement top-down control processes, while gamma activity is more likely to support bottom-up sensory processing (Miller et al., 2018). Regarding CAC, midfrontal theta power has been shown to be associated with conflict resolution, and to coordinate beta activity through cross-frequency coupling (Cohen, 2014; Duprez et al., 2020).

So far, most studies have evaluated FC in PD using resting-state fMRI (Baggio et al., 2015, 2014; Lopes et al., 2017; Skidmore et al., 2011; Wolters et al., 2019). The literature focusing on FC evaluated by (M)EEG and/or during cognitive tasks in PD is scarcer, although it would surely provide valuable insights on the neurophysiological alterations caused by the disease and its relationship with cognitive symptoms. While (M)EEG does not benefit from the same spatial resolution as fMRI, recent advances in cortical source reconstruction now enable the inference of cortical area long-range FC (Hassan and Wendling, 2018). One major advantage of (M)EEG techniques is their excellent temporal resolution (millisecond scale), which is fundamental when studying cognitive processes that are inherently fast and dynamic. For instance, CAC is a process that has obvious dynamic properties at the behavioral level: action selection and suppression are time-resolved processes allowing conflict resolution, and these aspects were usually masked by focusing on task-averaged behavioral performances in previous studies (van den Wildenberg et al., 2010).

Similarly to cognitive processes, FC is also time-dependent and brain networks dynamically rearrange themselves during resting state and tasks (Baker et al., 2014; Bola and Sabel, 2015; de Pasquale et al., 2016; Hassan et al., 2015; Kabbara et al., 2021; O'Neill et al., 2018, 2017) with consequences on behavior (Allen et al., 2018). Several new methods now allow investigating how inter-regional communication varies with time (Sizemore and Bassett, 2018; Tabbal et al., 2021). Such methods would tremendously help in understanding how dynamic cognitive processes such as CAC unravel, and how those processes can be impaired in neurodegenerative diseases such as PD. In this study, we aimed at describing the spatio-temporal characteristics of the functional networks during CAC and to test whether impairments in such characteristics are found in PD patients. We use the example of a classic conflict task, the Simon task, paired with high-density EEG (HD-EEG, 256 channels) reconstructed at the cortical source level in a group of 10 PD patients and 10 HC. We combine the calculation of dynamic FC matrices with a dimension reduction method (independent component analysis, ICA) and micro-state metrics to investigate the time-varying changes in brain networks at the group- and subject-level. Microstates are quasi-stable topographical patterns that can be used to investigate EEG dynamics. Some metrics were defined to investigate the presence of these microstates at the subject-level (Lehmann et al., 2005, 1987). We propose to use these metrics to quantify, instead of microstates, the presence of functional networks at the single subject-level. Since the method that we used is

based on a sliding window approach of phase-based FC, we were therefore limited to the investigation of the gamma and beta frequency bands. This allowed us to identify and characterize the frequency-dependent networks underlying CAC in PD patients and HC.

## 2. Materials and methods

### 2.1. Participants

Ten patients (6 males, 4 females) diagnosed with idiopathic PD (Hughes et al., 1992), aged between 48-59 years (mean = 53.6, std = 4.2) and 10 HC (4 males and 6 females), aged between 45-57 years (mean = 52.8, std = 4.3) participated in this study (Table 1). Patients with major cognitive deficits (Montreal Cognitive Assessment [MoCA], <22) or with other past or present neurological (other than PD) or psychiatric pathology, as well as patients with deep brain stimulation, were not included in the study. The same criteria were used for HC. Global cognitive functioning was assessed in all participants using the MoCA (Nasreddine et al., 2005). Additional standardized tests were assessed for PD patients, representing several cognitive abilities. These tests included: the Symbol Digit Modalities Test (SDMT; Smith, 1982), the Digit span test (Wechsler, 1981), the Stroop test (Stroop, 1935), the judgment of line orientation test (Benton et al., 1978), the Boston naming test (Graves et al., 2004), as well as semantic fluency (animal names generation task in 60 seconds), and phonemic fluency (words generation task in 60 seconds).

All HC were recruited from the general population during public conferences and through participation calls. Patients were recruited at the University Hospital of Rennes, France during hospitalization for their usual care. All participants provided informed consent for participation in the study, which was approved by a national ethics committee review board (CPP ID-RCB: 2019-A00608-49; approval number: 19.03.08.63626).

### 2.2. Experimental task

In this study, we used a color version of the Simon task (Simon and Rudell, 1967) to investigate the changes in CAC associated with PD. Participants were seated at a distance of 80 cm from a 22 inches' computer screen. At the beginning of a trial, a central dark fixation cross was presented on a white screen, during a variable period (pseudo-randomly defined from 1750 ms to 2170 ms). Then, a blue or a yellow circle (3.9 cm diameter) was displayed either to the right or left side during 200 ms (Fig. 1). Participants were asked to press a left or right button according to the color of the circle displayed, while ignoring its location (color/side mapping was counterbalanced across participants). Participants had to respond within 1000 ms after stimulus offset. The location side of the colored circle stimulus could match (congruent) or not (incongruent) the side of the correct button press associated with the color. For example, when the color "blue" is mapped to the "right" button, the trial is congruent when a blue circle appears on the right side, and incongruent when it appears on the left side (Fig. 1).

**Table 1**
Demographic and clinical data. Data are presented as mean (range; sd).

| | PD patients | HC | Welch's t-test |
|---|---|---|---|
| *n* | 10 | 10 | |
| *Age (years)* | 53.6 (48-59; 4.2) | 52.8 (45-58; 4.3) | t = 0.42; df = 18; p = 0.68 |
| *Sex (F/M)* | 4/6 | 6/4 | - |
| *Laterality (L/R)* | 2/8 | 0/10 | - |
| *Education level (years)* | 13.4 (9-17; 2.8) | 14.4 (9-17; 2.7) | t = -0.8; df = 17.9; p = 0.43 |
| *Motor characteristics* | | | |
| *Disease duration (years)* | 9.1 (6-17; 3.2) | - | - |
| *Onset side (L/R)* | 5/5 | - | - |
| *UPDRS III ON (/132)* | 12.1(4-29; 6.6) | - | - |
| *UPDRS III OFF (/132)* | 40.9 (24-68; 12.6) | - | - |
| *Hoehn & Yahr ON (/5)* | 0.8 (0-2; 0.8) | - | - |
| *Hoehn & Yahr OFF (/5)* | 1.9 (1-2.5; 0.5) | - | - |
| *Schwab & England ON (/100)* | 94 (90-100; 5.2) | - | - |
| *Schwab & England OFF (/100)* | 76 (50-90; 12.6) | - | - |
| *Levodopa Daily Dose Equivalent (mg/d)* | 1535 (995-2204; 398.2) | - | - |
| *Cognitive characteristics* | | | |
| *MoCA (/30)* | 27.5 (26-30; 1.5) | 28.9 (26-30; 1.4) | t = -2.1; df = 18; p = 0.048 |
| *SDMT* | | | |
| *Number in 90 s (/150)* | 49.6 (43-67; 7.2) | - | - |
| *Error (/150)* | 0.9 (0-4; 1.4) | - | - |
| *Digit Span* | | | |
| *forward (/9)* | 5.9 (5-7; 0.9) | - | - |
| *backward (/9)* | 4.8 (3-6; 0.9) | - | - |
| *Stroop task* | | | |
| *interference time (s)* | 49 (38-72; 9.7) | - | - |
| *interference errors (n errors)* | 0.5 (0-2; 0.7) | - | - |
| *Judgement of line orientation (/30)* | 26.6 (24-29; 1.6) | - | - |
| *Boston naming test (/15)* | 12.3 (10-15; 1.6) | - | - |
| *Verbal fluency* | | | |
| *Semantic (animals in 60s)* | 21.2 (15-30; 5.2) | - | - |
| *Phonemic (P in 60s)* | 16.9 (11-24; 4.7) | - | - |
| *Simon task* | | | |
| *Overall RT* | 520 (103) | 580 (126) | t = -1.7 ; df = 1 ; p = 0.1 |
| *Congruent RT* | 497 (66) | 556 (81) | t = -1.8 ; df = 17 ; p = 0.09 |
| *Incongruent RT* | 544 (64) | 606 (95) | t = -1.7 ; df = 16 ; p = 0.11 |
| *Overall accuracy* | 0.96 (0.2) | 0.96 (0.2) | t = -0.5 ; df = 18 ; p = 0.6 |
| *Congruent accuracy* | 0.98 (0.02) | 0.99 (0.01) | t = -1.4 ; df = 12 ; p = 0.19 |
| *Incongruent accuracy* | 0.94 (0.04) | 0.93 (0.05) | t = -0.18 ; df = 17 ; p = 0.86 |

UPDRS : Unified Parkinson's Disease Rating Scale; SDMT : Symbol Digit Modality Test; Levodopa equivalent daily dose was calculated according to Tomlinson et al. (2010).

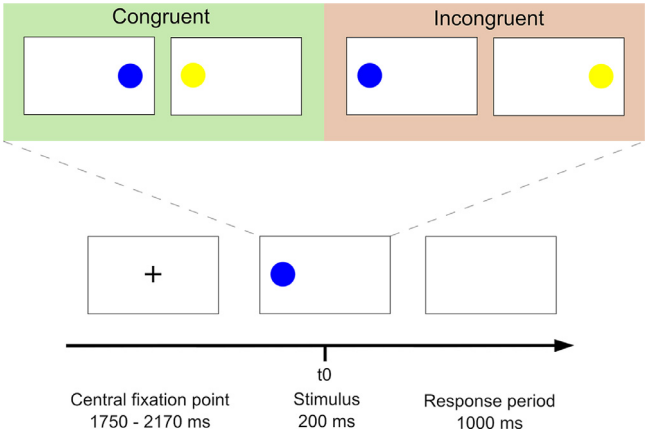



**Fig. 1.** Overview of the Simon Task. The central fixation point was displayed randomly from 1750 to 2170 ms, with a 30 ms step. Then, the stimulus display lasted 200 ms. Participants had 1000 ms to answer by pressing the button. Two conditions could occur: congruent, when color and location of the circle led to the same response; and incongruent, when color and location didn't lead to the same response. (For interpretation of the references to color in this figure legend, the reader is referred to the web version of this article.)

After a 60-trials training session, participants performed 10 blocks of 60 trials, with short pauses between blocks and a longer pause every three blocks to check EEG electrodes' impedance. In total, 600 trials were performed with 300 congruent and 300 incongruent trials with a pseudo-randomized display.

### 2.3. Data acquisition and preprocessing

EEG signals were recorded using a HD-EEG system (EGI, Electrical Geodesic Inc., 256 channels), with a sampling frequency of 1000 Hz. 199 electrodes were kept, removing most of the jaw and neck electrodes, as shown in the channel file available in the GitHub repository (see section 2.8). EEG preprocessing was performed manually using the Brainstorm toolbox (Tadel et al., 2011). Preprocessing was performed as follows. First, DC offset removal was applied. Second, a notch filter at 50 Hz and a band-pass filter of 1-100 Hz were applied. Third, signals were visually inspected, and bad channels were removed before being interpolated using Brainstorm's default parameters. Fourth, Independent Component Analysis (ICA) was used to remove eye blinks and muscle artifacts. Fifth, we segmented the recorded signals into epochs from -700 ms to 1200 ms relative to the stimulus onset. Finally, a visual inspection was performed to manually reject epochs with excessive remaining noise. For EEG analyses, we focused on correct incongruent trials only, because they are associated with efficient control in a condition of strong conflict and because congruent situations could involve different networks. Thus, comparing networks in two conditions for PD and HC would be challenging. As a result, out of originally 300 incongruent trials, 174 incongruent trials per subject on average (STD = 49.2) were kept for further analyses because of the removal of errors, the absence of response, or because of remaining artifacts.

After EEG preprocessing, several steps were applied to identify the dynamic brain network states in all participants (HC and PD), as summarized in Fig. 2 and explained below.

### 2.4. EEG source connectivity

#### i. Forward Model

Following the equivalent current dipole model, EEG signals measured from Q channels can be expressed as linear combinations of P time-varying current dipole sources as follows:

$$X(t) = G.S(t) + N(t) \quad (1)$$

Where $G(Q \times P)$ represents the forward model, often called the lead field matrix, and $N(t)$ denotes the additive noise. The lead field matrix is computed from a realistic head model along with the position of electrodes. Here, we used the Boundary Element Method (BEM) head model fitted to the ICBM MRI template (Kötter et al., 2001), downloaded from https://www.mcgill.ca/bic/software/tools-data-analysis/anatomical-mri/atlases/icbm152lin using the OpenMEEG toolbox (Gramfort et al., 2010), and used the Electrical Geodesic Inc (EGI) configuration for the EEG electrodes.

#### ii. Inverse Solution: wMNE

The EEG inverse problem consists in estimating the unknown parameters of dipolar source S(t) at the cortical level (position, orientation, and magnitude), from the measured EEG signals X(t) at the scalp level. Here, we used the Destrieux atlas parcellation (148 ROIs) (Destrieux et al., 2010) to locate cortical sources, and constrained their orientation normally to the cortical surface (Dale and Sereno, 1993). Therefore, the EEG inverse problem was reduced to the estimation of sources magnitude:

$$S(t) = W.X(t) \quad (2)$$

To compute the inverse matrix W, we used the weighted minimum norm estimate (wMNE) (Lin et al., 2006) method, that compensates the tendency of the classical minimum norm estimate (MNE) (Hämäläinen and Ilmoniemi, 1994) to favor weak and surface sources:

$$W = BG^T(GBG^T + \alpha C)^{-1} \quad (3)$$

where B is the diagonal weighting matrix (inversely proportional to the norm of lead field vectors), G is the lead field matrix, $\alpha$ is the regularization parameter (based on signal to noise ratio: $\alpha = 1/\mathrm{SNR}$, and C is the noise covariance matrix (calculated from our 700 ms pre-stimulus baseline). Here, we used the Matlab function implemented in the Brainstorm toolbox to compute wMNE. The SNR was set to 3, and the depth weighting value to 0.5 (default values).

#### iii. Dynamic Functional Connectivity: PLV - sliding window

Several approaches have been proposed to compute functional connectivity between reconstructed regional time series. In this study, we used the phase-locking value (PLV) method (Lachaux et al., 2000). Since we aimed to assess functional connectivity dynamics, we chose the sliding window approach defined by its length $\delta$ with an overlapping step $\Delta$. Hence, for each correct incongruent trial, PLV measures the phase synchronization between two signals $x(t)$ and $y(t)$ within each temporal window t:

$$PLV(t) = \left| \frac{1}{\delta} \int_{t-\frac{\delta}{2}}^{t+\frac{\delta}{2}} e^{j(\varphi_y(t)-\varphi_x(t))} d\tau \right| \quad (4)$$

where $\varphi_y(t)$ and $\varphi_x(t)$ are the instantaneous phases of signals y(t) and x(t), respectively derived from the Hilbert transform.

The choice of temporal window length was based on (Lachaux et al., 2000), where it is recommended to consider at least 6 cycles at the frequency band of interest as a compromise between temporal and spatial accuracy. In this study, we conducted our analysis separately in both the beta [12-25 Hz] (central frequency: Cf = 18.5 Hz) and gamma bands [30-45 Hz] (central frequency: Cf = 37.5 Hz). Thus, we chose the smallest window length equals to 6/Cf, that is 320 ms for the beta band and 160 ms for the gamma band. We considered a 90% overlap between consecutive windows to track fast neural activity. Therefore, the total number of windows over the whole trial duration was $nWinds = 49$ windows for the beta band, and nWinds = 109 windows for the gamma band, and the output dimension of the dynamic functional connectivity (dFC) matrix was nROIS x nROIS x nWinds for each subject trial. Since the choice of the number of cycles and window length remains subjective, we tested how the networks estimated from one dataset were similar with varying number of cycles (4, 6 or 8) and overlap between windows (70, 80 or 90%). We extracted the networks following the steps

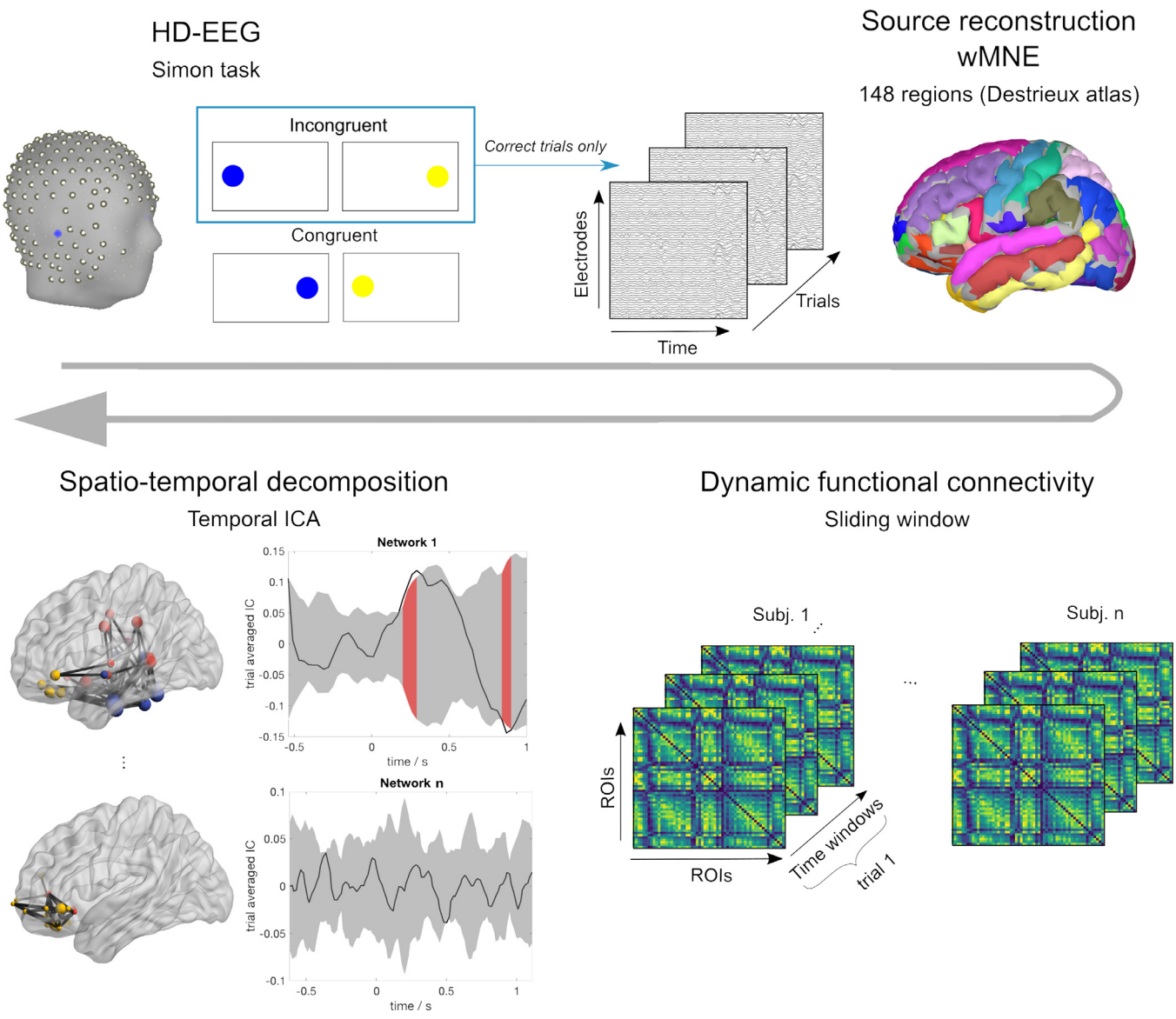



**Fig. 2.** Dynamic FC pipeline used in our study. First, HD-EEG data was recorded during the Simon task (only correct incongruent trials were considered). After preprocessing, cortical-level sources were reconstructed using the weighted Minimum Norm Estimate (wMNE) and the Destrieux atlas (148 Regions of Interests, ROIs). Then, dynamic functional connectivity (dFC) was estimated for each subject and trial using a sliding window. Phase Locking Value (PLV) was used to quantify the statistical coupling between ROIs. Finally, the temporal Independent Component Analysis (tICA) was applied on the dFC tensor to extract dynamic brain network states, including spatial network maps and temporal activity. A null distribution was generated to assess the temporal moments of significant modulation for each of the extracted states (as highlighted in red). (For interpretation of the references to color in this figure legend, the reader is referred to the web version of this article.)

described below, and correlated FC matrices between the different analyses with varying number of cycles and overlap. This analysis showed that networks highly correlated with each other when varying overlap, but keeping the same number of cycles (see Supplementary Figure 1), however correlation decreased when changing the number of cycles. Considering those results, we chose to follow the recommendation of Lachaux et al. (2000) and kept the number of 6 cycles for analyses, and the value of 90% for overlap.

### 2.5. Dynamic brain network states (dBNS)

*i. Temporal Independent Component Analysis (tICA): JADE*

For each subject's correct incongruent trial, the dFC tensor can be unfolded into a 2D matrix of dimension [nROIS(nROIS – 1)/2 x nWinds] due to symmetry. Then, the resultant dFC matrices of all trials and subjects of both groups were concatenated along the temporal dimension to generate a dFC matrix denoted M.

Since we aimed to summarize and extract the most relevant time-varying connectivity patterns in M, this problem can be formulated as follows:

$$M = A \times B \tag{5}$$

Where A is the mixing matrix that represents the 'k' spatial maps of dominant brain network states, and B describes their temporal evolution. Among the existing decomposition and clustering techniques, we derived the dynamic Brain Network States (dBNS) using temporal Independent Component Analysis (tICA) adopted by several previous studies (O'Neill et al., 2017; Yaesoubi et al., 2015). This technique assumes maximal independence between the time courses of the extracted dBNS. Here, tICA was performed using the JADE algorithm (Joint Approximate Diagonalization of Eigen-matrices) (Cardoso and Souloumiac, 1993; Rutledge and Jouan-Rimbaud Bouveresse, 2013). Briefly, JADE applies the Jacobi technique to optimize contrast functions based on high statistical order (Fourth Order: FO) cumulants of the data. One advantage

of JADE compared to other ICA methods (FastICA, infomax, ...), in our situation, is its high robustness for small sample sizes: Tabbal et al., 2021 showed that group-subject similarity was above 90% when there were only 5 subjects, and 100% with as few as 7 subjects. Here, the JADE function in Matlab was used (The Mathworks, USA, version 2019a).

*ii. Number of states selection*

Determining the optimal number of states to be extracted by tICA is a crucial issue for most decomposition and dimensionality reduction methods (Cong et al., 2013; Mørup and Hansen, 2009). Here, we used the DIFFIT (difference in data fitting) method based on the goodness-of-fit approach (Timmerman and Kiers, 2000; Wang et al., 2018), previously used by recent studies (Tabbal et al., 2021; Tewarie et al., 2019; Zhu et al., 2020). DIFFIT is calculated based on the following equations:

$$Fit(J) = -\frac{|M - M'(J)|L_F}{|M|_F} \tag{6}$$

$$DIFFIT(J) = \frac{Fit(J) - Fit(J-1)}{Fit(J+1) - Fit(J)} \tag{7}$$

Where M is the original concatenated dFC matrix to be decomposed, and M' is the reconstructed matrix after tICA decomposition at the number of states J , and $\|F$ is the Frobenius norm. We varied J from 3 to 10 states, then chose the number of states J resulting in the largest DIFFIT value. We applied the DIFFIT method on the dFC matrix of each subject separately, then averaged the obtained DIFFIT values across subjects to obtain an average of 6 dynamic brain network states (dBNS) for the beta band (mean = 5.6) and 5 for the gamma band (mean = 5). We did not apply a subject-specific choice of the number of components, since ICA searches for ICs on the concatenated data of all participants. Furthermore, subject-specific ICA with subject-specific number of components would lead to challenging comparisons since all participants would not have the same number of networks to compare.

*iii. Significant task-modulated states*

An additional step was followed to automatically select, from all extracted dBNS, those that were significantly modulated by the task. First, we built an empirical null distribution through the generation of a surrogate time course based on a sign-flipping permutation following the procedure detailed in previous studies (Hunt et al., 2012; O'Neill et al., 2017; Tabbal et al., 2021; Winkler et al., 2014). Briefly, at each permutation (n = 10000), a random number of subjects had the sign of their contributions to the ICs flipped. The null hypothesis here is that if the IC is not task-related, sign-flipping will not affect the magnitude of IC's time courses. However, if the IC is modulated by the task (stimulus onset) robustly across subjects, then trial-averaged ICs time courses changes in connectivity would be maintained while this would not be the case for the null distribution.

A dBNS was considered as significant if its corresponding time course fell outside the null distribution at any time point of the trial-averaged IC time course. 2-tailed distribution was allowed, followed by a Bonferroni correction accounting for multiple comparisons across the extracted dBNS (see (O'Neill et al., 2018, 2017) for details). Consequently, a set of $NS$ significant states were obtained.

### 2.6. Between-group statistical differences

Finally, we intended to quantify the statistical differences between HC and PD groups regarding the dBNS defined by tICA. To achieve this, we used a back-fitting approach applied to EEG microstates, previously used at the sensor-level (Khanna et al., 2015; Michel and Koenig, 2018), as described below and illustrated in Fig. 3.

*i. Back-Fitting*

First, all selected $NS$ states were assigned separately to all participants (HC and PD patients) and to every temporal window of all individual dFC, using the approach proposed by (Ville et al., 2010) in the context of classical scalp-level 'microstates'. The spatial similarity (correlation) was calculated between the dFC map at every temporal window and each of the dBNS. Then, using a 'winner-takes-all' approach, each temporal window was labeled with the best-fitting dBNS: only the dBNS with the highest correlation with the dFC was kept. Therefore, we obtained a temporal dBNS sequence for each individual dFC for both groups.

*ii. Network States Metrics*

Several features of the various dBNS, originally coming from the microstate literature, can be computed separately for each HC and PD subjects (Lehmann et al., 2005). These metrics will be referred to as network states metrics for the rest of the paper in order to avoid potential confusions in interpretation. Our features of interest were:

- Average lifespan (or mean duration; in seconds). The lifespan of a dBNS was calculated as the average time during which a given dBNS remains stable for successive segments (Lehmann et al., 1987).
- Fraction coverage time (in percentage between 0 and 1). The coverage is defined as the ratio of the time frames for which a given dBNS is dominant relative to the total recording duration (Lehmann et al., 1987).
- Frequency of occurrence (in Hz). The frequency of occurrence represents the number of unique appearances of the dBNS per second, independently of its duration (Lehmann et al., 1987).
- Global Explained Variance (GEV; in percentage between 0 and 1). The GEV of a dBNS is the percentage of the total variance explained by this dBNS (Brodbeck et al., 2012).
- Transition probabilities. The transition probabilities are defined, for each pair of states, by the probability of occurrence of the considered transition given all transitions. (Lehmann et al., 2005).

### 2.7. Statistical analysis

All statistical analyses were performed using R version 4.0.2 (R Core Team, 2020) implemented with the *lme4* package for mixed model analyses (Bates et al., 2015).

*i. Behavior*

RT and accuracy are the variables measured during the Simon task. Comparing congruent and incongruent RT of correct responses provides an estimate of the congruence effect that informs about the additional time needed to solve conflict. Incongruent trials are typically associated with increased RT and decreased accuracy. In addition to the analysis of the congruence effect, behavioral data were also analyzed in light of the activation-suppression model (Ridderinkhof, 2002), which informs about the temporal characteristics of cognitive action control. These are based on distributional analyses that measure impulsive action selection (incongruent accuracy for the fastest trials) and suppression (slope value of the congruence effect for the slowest trials). A complete description of the model and analysis steps can be found in van den Wildenberg et al. (2010) and in Duprez et al. (2017). Briefly, RT are increasingly ordered and divided into 7 bins. Accuracy and congruence effect (incongruent RT - congruent RT) are then calculated for those 7 bins resulting in two different representations : conditional accuracy functions and delta plots, respectively. The activation-suppression model postulates that incongruent accuracy of the first bin (fastest trials) informs about impulsive action selection, while the slope between the two last bins of the delta plots informs about selective suppression of such impulsive actions.

The effect of congruence and group on RT and accuracy were first broadly analyzed by using linear and non-linear mixed models, respectively. In both cases, congruence and group were added as fixed factors, while a random slope and intercept was allowed for each subject. RT were log-transformed for increased compliance with the model's assumptions in that case. The formulas used for the models were the following:

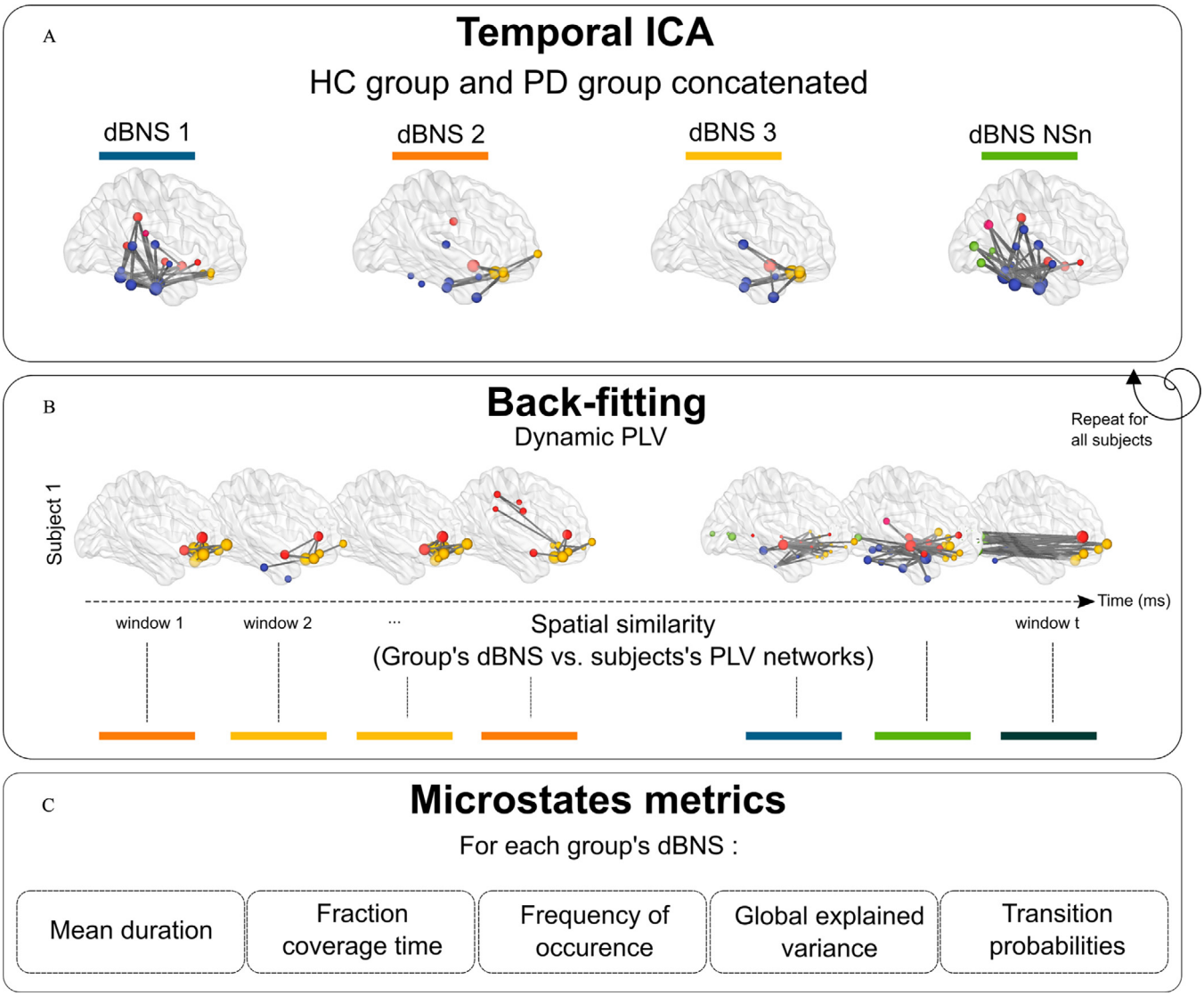



**Fig. 3.** A. Temporal ICA applied to the concatenation of the HC and PD groups. B. Back-Fitting approach assigns PLV network at each temporal window with one of all the ICA networks (microstate) having the highest spatial similarity value (strongest correlation). This was applied on all HC and PD subjects, followed by a calculation of the main network states metrics as shown in C.

- RT model

$$\text{Model} = \text{lmer}(\log(\text{RT}) \sim \text{condition x group} + (\text{condition}|\text{subject}), \text{data} = \text{data}) \quad (8)$$

- Accuracy model :

Model = glmer(accuracy ~ condition x group + (condition|subject), family = binomial, glmerControl(optimizer="bobyqa"), data = data) (9)

Fixed effects significance were computed through the *Anova* function of the {car} package (Fox and Weisberg, 2019) that calculates type II Wald chi-square tests. Marginal ($m$R$^2$) and conditional ($c$R$^2$) R$^2$ were calculated using the {MuMin} package (Barton, 2009).

Average first bin incongruent accuracy and last slope values of conditional accuracy and delta plots were directly extracted from subjects in both groups and compared using Welch's t test and are reported with effect size (Cohen's d).

*ii. Network states metrics*

To quantify the differences between HC and PD groups in terms of network states parameters (mean duration, fraction coverage time, frequency of occurrence, GEV, and transition probabilities), statistical tests were performed

### 2.8. Code availability

All the Matlab and R codes used for source reconstruction, dFC, tICA, backfitting and microstate metrics, as well as all subsequent statistical analyses are publicly available at https://github.com/jduprez/EEGcog-control_dynFC_PD.

## 3. Results

This section first presents the behavioral results. Then, the EEG network results are divided in group-level results, presenting the significant dBNS derived from tICA, and subject-level results, relative to each subjects' network states metrics of significant dBNS.

### 3.1. Behavioral results

The typical congruence effect was found, showing increased RT ($X^2$ = 119, p < 0.0001; $m$R$^2$ = 0.1; $c$R$^2$ = 0.5) and decreased accuracy

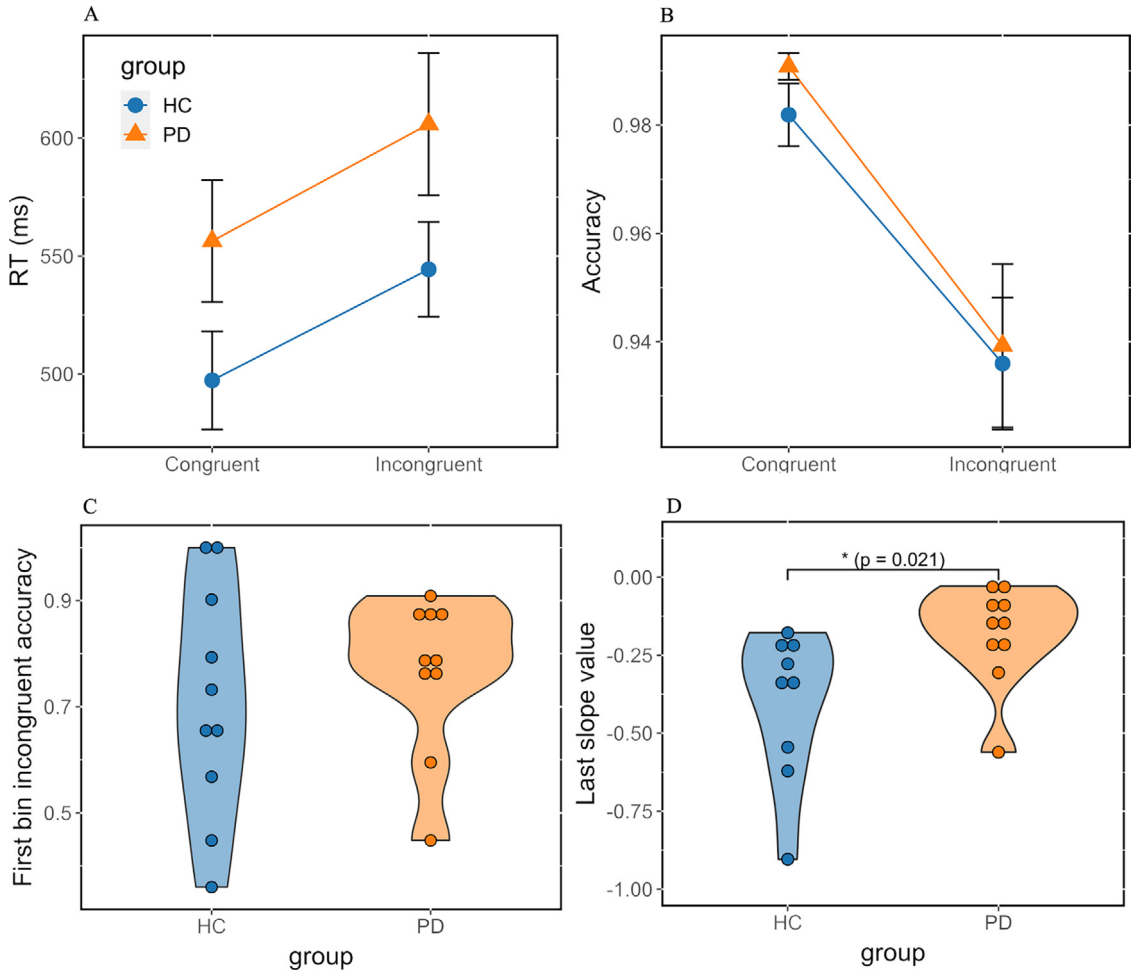



**Fig. 4.** Average RT (A) and accuracy (B) as a function of congruence in both groups. Error bars represent standard error of the mean. Impulsive action selection is denoted by group-specific violin plots showing accuracy of the first incongruent bin (C) of conditional accuracy function. The strength of selective inhibition is represented by group-specific violin plots showing the last slope value (D) of delta plots.

($X^2$ = 51.6, p < 0.0001; $mR^2$ = 0.18; $cR^2$ = 0.32) in the incongruent condition (Fig. 4A and B). Although PD patients seemed slower than HC regardless of congruence, this effect was not significant ($X^2$ = 2.9, p = 0.09). PD patients were also overall similarly accurate as compared to HC ($X^2$ = 0.04 p = 0.8). The congruence effect was not significantly different between groups, both for RT ($X^2$ = 0.4, p = 0.5) and accuracy ($X^2$ = 1.5, p = 0.2). Conditional accuracy functions revealed the classic pattern of increased accuracy with RT (see supplementary figure SF2A-B). Accuracy of the first bin in the incongruent condition reflects impulsive action selection (Fig. 4C), and did not significantly differ between PD patients and HC (t = -0.23, p = 0.51). Inspection of delta plots (see supplementary Figure SF2C) also exhibited the typical decreasing pattern of the congruence effect associated with the Simon task. The last slope of delta plots informs on the strength of selective inhibition of inappropriate responses (Fig. 4D). In line with our hypothesis, PD patients had a significantly flatter slope, indicative of reduced proficiency in inhibiting automatic responses (t = -2.61, p = 0.02; Cohens' d = 1.2).

### 3.2. Group-level results – Significant task-modulated dBNS

In this section, we focus on the dynamics of the brain networks derived at the group-level from tICA. In the following, Bi denotes the dBNSi extracted in the beta band, and Gj the dBNSj extracted in the gamma band. Only the dBNS that were significant following permutation testing are presented here. However, all tICA-derived dBNS (significant or not) and their dynamic modulation (along with the null distribution) can be found in Supplementary Figures SF3-4. All dBNS are presented in the order in which they were derived by tICA (e.g. dBNS B1 will be the first significant dBNS found by tICA in the beta band). Our results show that, in the beta band, three significant dBNS were identified. In the gamma band, five significant dBNS were derived. The spatiotemporal dynamics of beta and gamma dBNS are illustrated in Figs. 5 and 6, respectively. Since we aimed at tracking the evolution of the task-related components, we have plotted on the same time axis each group-specific dBNS and marked the corresponding duration for which they had a significant modulation. For the sake of visualization, we plotted the top 0.5% edges relative to the total number of unique possible connections, i.e., the top 55 edges per network. Using this threshold, in order to globally describe the integrated brain regions and characterize functional networks, we calculated the percentage of nodes with respect to the total number of ROIs, for each of the five macroscopic regions (F: Frontal, T: Temporal, P: Parietal, O: Occipital, and C: Cingulate/insula). In the description of the networks, only some of the nodes involved in the networks are discussed for clarity and are summarized based on larger regions they belong to. However, the reader can refer to Supplementary Table ST1 for a complete description of the Destrieux atlas regions involved in the networks, following the thresholding we previously described.

#### 3.2.1. Beta band

In the beta band, B1 (Fig. 5A) was significantly modulated by the task during two different periods, before and after the both groups av-

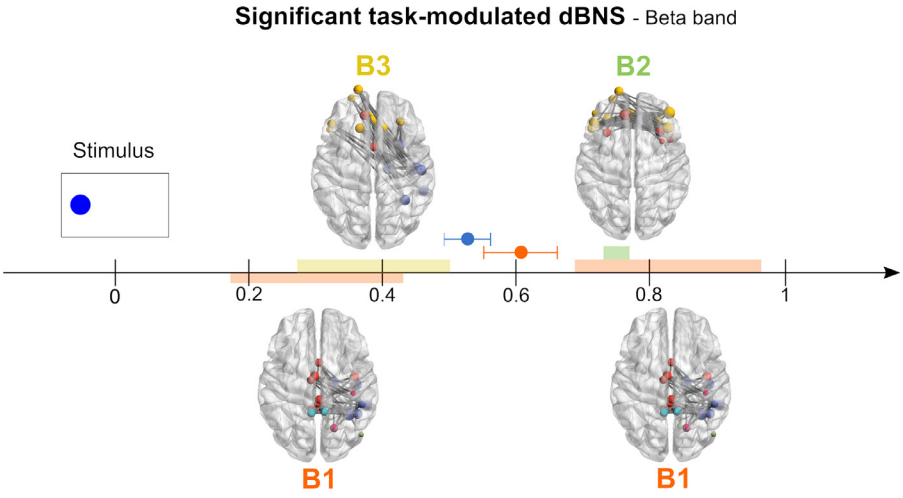



**Fig. 5.** Spatiotemporal dynamics of the significant task-modulated dBNS in the beta band. Time 0 corresponds to stimulus onset. Each significant dBNS is illustrated as a brain network with a specific color. All brain networks were thresholded (only the top 0.5% edges are shown) for visualization. Node size is proportional to the degree (number of edges incident to a node). A color code is attributed for all nodes belonging to the same brain lobe (yellow for frontal, blue for temporal, light blue for parietal, green for occipital, and red for cingulate and insula). For each dBNS, we indicated the temporal duration during which it is significantly modulated by the task (positively modulated are plotted above the time axis, negatively modulated are plotted below the time axis). Overlaid data point corresponds to the average correct incongruent RT ± sd of all trials (blue corresponds to HC, and orange to PD patients). Below, the percentages of nodes relative to each brain lobe are illustrated on the colored bars for each state. The reader can refer to Supplementary Figure SF3 for a detailed representation of the networks (top, left, and right views) with the corresponding averaged-trial temporal signals plotted over the whole temporal duration along with the null distribution to reveal the temporal significance. In supplementary table ST1, the labels of the activated Destrieux ROIs are highlighted. (For interpretation of the references to color in this figure legend, the reader is referred to the web version of this article.)

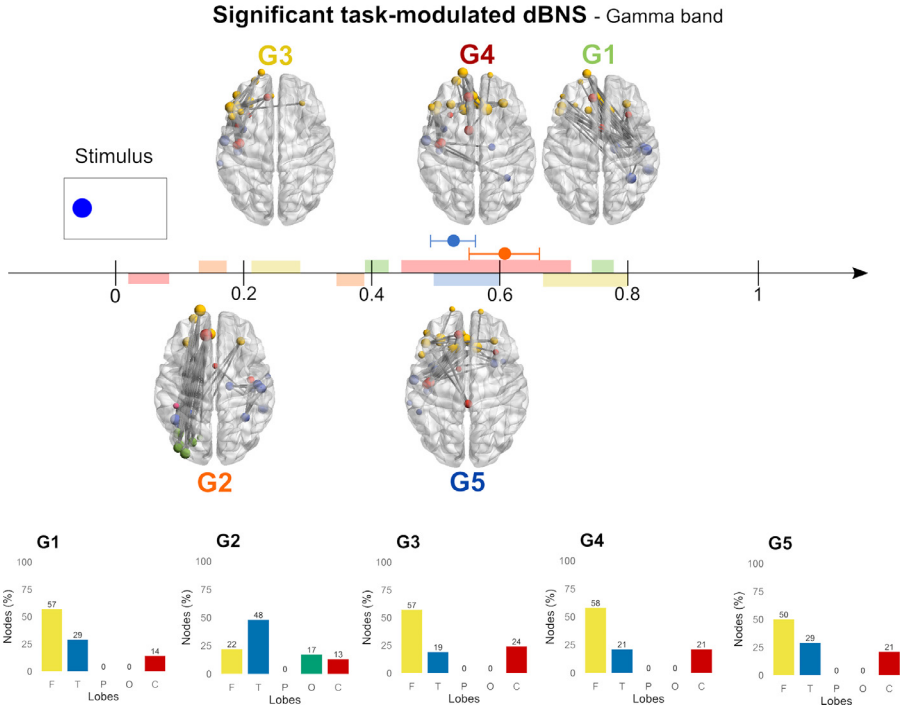



**Fig. 6.** Spatiotemporal dynamics of the significant task-modulated dBNS in the gamma band. The time 0 s corresponds to the stimulus offset. Each significant dBNS is illustrated as a brain network with a specific color. All brain networks were thresholded for visualization. Spheres of different sizes proportional to their strength represent the activated brain nodes. A color code is attributed for all nodes belonging to the same brain lobe (yellow for frontal, blue for temporal, light blue for parietal, green for occipital, and red for cingulate and insula). For each state, we indicated the temporal duration on which it is significantly modulated by the task (positively modulated are plotted above the time axis, negatively modulated are plotted below the time axis). Overlaid data point in black corresponds to the average correct incongruent RT ± sd of all trials (blue corresponds to HC, and orange to PD patients). Below, the percentages of nodes relative to each brain lobe are illustrated on the colored bars for each state. The reader can refer to Supplementary Figure SF3 for a detailed view representation of the network (top, left, and right) with the corresponding averaged-trial temporal signals plotted over the whole temporal duration along with the null distribution to reveal the temporal significance. In supplementary table ST1, the labels of the activated Destrieux ROIs are highlighted. (For interpretation of the references to color in this figure legend, the reader is referred to the web version of this article.)

eraged RT (HC : 544 ms, sd = 64; PD : 606 ms, sd = 95), ranging from 170 to 420 ms, with a decrease in connectivity; then from 680 to 970 ms showing increased connectivity. This network mainly involved connections in the cingulate and insular regions (40%), including left and right posterior cingulate, right inferior insula and pericallosal areas. B1 also included right temporal lobe nodes (35%), with inferior temporal, parahippocampal and fusiform regions. Finally the parietal lobe was involved (15%) bilaterally around the parieto-occipital sulcus, as well as the occipital lobe (10%) with inferior occipital regions. No frontal regions were found in B1.

A second dBNS B2 was significantly modulated by the task with an increase in connectivity after the average RT, ranging from 740 to 770 ms. B2 involved essentially connections in the frontal lobe (74%), represented by inferior frontal, frontopolar and orbitofrontal nodes bilaterally, and in the cingulate and insular regions (26%), with left and right anterior cingulate and anterior insula nodes. No nodes were found in other lobes.

Finally, a third dBNS B3 was significantly modulated by the task, having greater connectivity before averaged RT, from 260 to 490 ms. This dBNS involved interhemispheric connections between the frontal

lobe (61%), with left inferior frontal and bilateral orbitofrontal and frontopolar regions, and the temporal lobe (28%), represented by right-sided superior and inferior temporal as well as parahippocampal regions. B3 also involved the cingulate lobe (11%), with left anterior cingulate and right subcallosal nodes. No parietal or occipital nodes were found in B3.

#### 3.2.2. Gamma band

In the gamma band, five dBNS were identified (Fig. 6) with an overall more overlapping pattern than within the beta band. First, G1 was significantly modulated by the task with increased connectivity before (from 390 to 420 ms)and after (from 740 to 770 ms) the average RT. G1 consisted mostly in frontal nodes (57%), predominantly in the left hemisphere, including inferior frontal, frontopolar, frontomarginal and orbital regions. Frontal nodes were highly connected with right temporal areas (29%) represented by superior and inferior temporal areas, as well as fusiform and parahippocampal regions. G1 also included deeper nodes (14%), including the left anterior cingulate and right subcallosal and anterior insula regions.

A second dBNS, G2, was significantly modulated by the task and had increased connectivity from 130 to 160 ms and decreased connectivity from 360 to 390 ms. G2 was characterized mostly by long range left-sided connections involving the frontal lobe (22%), with frontomarginal, frontopolar and orbitofrontal regions, and the occipital lobe, with middle and inferior occipital regions. The temporal lobe was the most represented (48%) with bilateral nodes involving superior temporal, fusiform and parahippocampal nodes. Finally, cingulate and insular regions were found in G2 (13%), with anterior cingulate and inferior insula nodes.

A third dBNS G3 showed a significant increase in connectivity from 210 to 280 ms and a decrease in connectivity after the average RT from 660 to 800 ms. G3 was essentially left-sided and involved the frontal lobe (57%) with inferior frontal, frontopolar, frontomarginal and orbitofrontal regions. G3 was also represented by nodes in the cingulate and insular areas (24%) with the anterior cingulate and anterior, central, and inferior insula. Temporal nodes were also found in G3 (19%) with superior and middle temporal regions.

G4 was significantly modulated by the task during two time periods with a decrease in connectivity observed from 20 to 70 ms and an increase in connectivity from 440 to 710 ms overlapping with both groups' average RT. G4 involved bilateral frontal nodes (58%) including inferior frontal, frontomarginal, frontopolar and orbitofrontal regions. The temporal lobe was also involved in G4 (21%), mostly in the left hemisphere, with superior temporal, fusiform and parahippocampal regions. The cingulate and insular regions were also found in G4 (21%) and included only left-sided regions with anterior cingulate, and anterior, central, and inferior insular nodes.

Finally, a fifth dBNS G5 was significantly modulated by the task with decreased connectivity observed from 500 to 600 ms, overlapping with G4. G5 involved bilateral frontal nodes including frontopolar and orbitofrontal regions. Bilateral temporal regions (29%) were also found in G5 with superior, inferior and middle temporal areas. G5 was also represented by cingulate and insular nodes (21%) including anterior and posterior cingulate regions as well as anterior and inferior insular areas.

### 3.3. Subject-level results - network states metrics analyses

As described in the Materials and Methods section, several network states metrics were computed for all subjects in both the beta and gamma bands, before performing the statistical analysis to quantify potential significant differences between groups. These are based on correlation between the dFC matrices with the dBNS, to determine, at any given time, which dBNS corresponds the most (has the highest correlation value) to the current network. Correlations between all dBNS were performed with the dFC matrices of all subjects. The metrics computed thereafter included (i) average lifespan, (ii) frequency of occurrence, (iii) fraction coverage time, (iv) global explained variance, and (v) transition probabilities. These results are presented in Fig. 7 for the beta band, and in Fig. 8 for the gamma band.

First, in the beta band, it can be noticed that the most represented network at the subject level for both groups was B2 (Fig. 7). This was evident for all the computed metrics. However, we found no difference in either metrics between PD patients and HC (all p-values > 0.05). It is worth noting that, overall, the dBNS that were significantly modulated by the task for the longest periods at the group-level (see section 3.2.1) were the least represented at the subject-level. Regarding transition probability, although it seemed that PD patients showed a greater probability of transition between B2 and B4, the effect wasn't significant ($p = 0.037$). As a whole, these results suggest that all the networks derived from tICA were equally represented in both groups.

Regarding the gamma band, results of the comparison of network states metrics are displayed in Fig. 8. The dBNS G1 was the most represented at the subject-level in terms of microstates metrics. We found no differences between groups relative to G1 metrics (all $p > 0.05$). Although Fig. 8 suggests that G5 was mostly found in PD patients and not in HC, this was not supported by statistical testing (all p-values > 0.05). No differences were found either between groups regarding transition probability. Similarly to the case of the beta band, the dBNS that were significantly modulated by the task during the longest period at the group-level (G3, G4), were not the most represented at the subject-level. Globally, these results suggest that gamma networks were also equally represented in both groups.

### 3.4. Correlation with behavioral/clinical data

Finally, we conducted correlations between behavioral data and EEG results (all scatterplots available in supplementary Figures SF5 to SF9). The only significant correlation between behavioral EEG results was a positive correlation between fast response accuracy and the global explained variance of the B1 dBNS ($R = 0.47$, $p = 0.036$). This correlation suggests that an increase in B1 global explained variance was associated with an increase in fast response accuracy. However, this correlation should be interpreted with caution since this was the only significant one between network metrics and behavioral results. We also conducted correlations with age, education level, and MoCA scores. We found significant correlations between MoCA and G1 average lifespan ($R = 0.59$, $p = 0.006$), with G1 fraction coverage time ($R = 0.58$, $p = 0.007$), with G1 frequency of occurrence ($R = -0.59$, $p = 0.006$), and with G1 global explained variance ($R = 0.59$, $p = 0.006$). G1 was also associated with education level regarding average lifespan ($R = 0.51$, $p = 0.02$), fraction coverage time ($R = 0.51$, $p = 0.02$) and frequency of occurrence ($R = -0.5$, $p = 0.03$). These correlations suggest that prolonged presence of G1 was associated with better MoCA scores and higher education level. Other correlations with gamma dBNS metrics were significant, but most probably spurious due to the occurrence of excessive 0 values (see SF5-6). Regarding the beta band, we found significant correlations between education level and B2 average lifespan ($R = 0.61$, $p = 0.005$) and B2 fraction coverage time ($R = 0.59$, $p = 0.006$), suggesting that increased presence of B2 was associated with higher education level. Similarly to the gamma band, other significant correlations were found but were only driven by a dominance of 0 values (see SF8). All other correlations were not significant.

## 4. Discussion

In this study, we aimed to explore i) how cognitive action control is associated with dynamically reconfiguring functional connectivity networks, and ii) how these dynamic structures are linked to PD-related alterations in CAC, as compared to healthy subjects. We used scalp HD-EEG recorded from 10 HC and 10 PD patients during a Simon task, and estimated source-reconstructed cortical functional networks within two frequency bands (beta and gamma). We applied a combination of

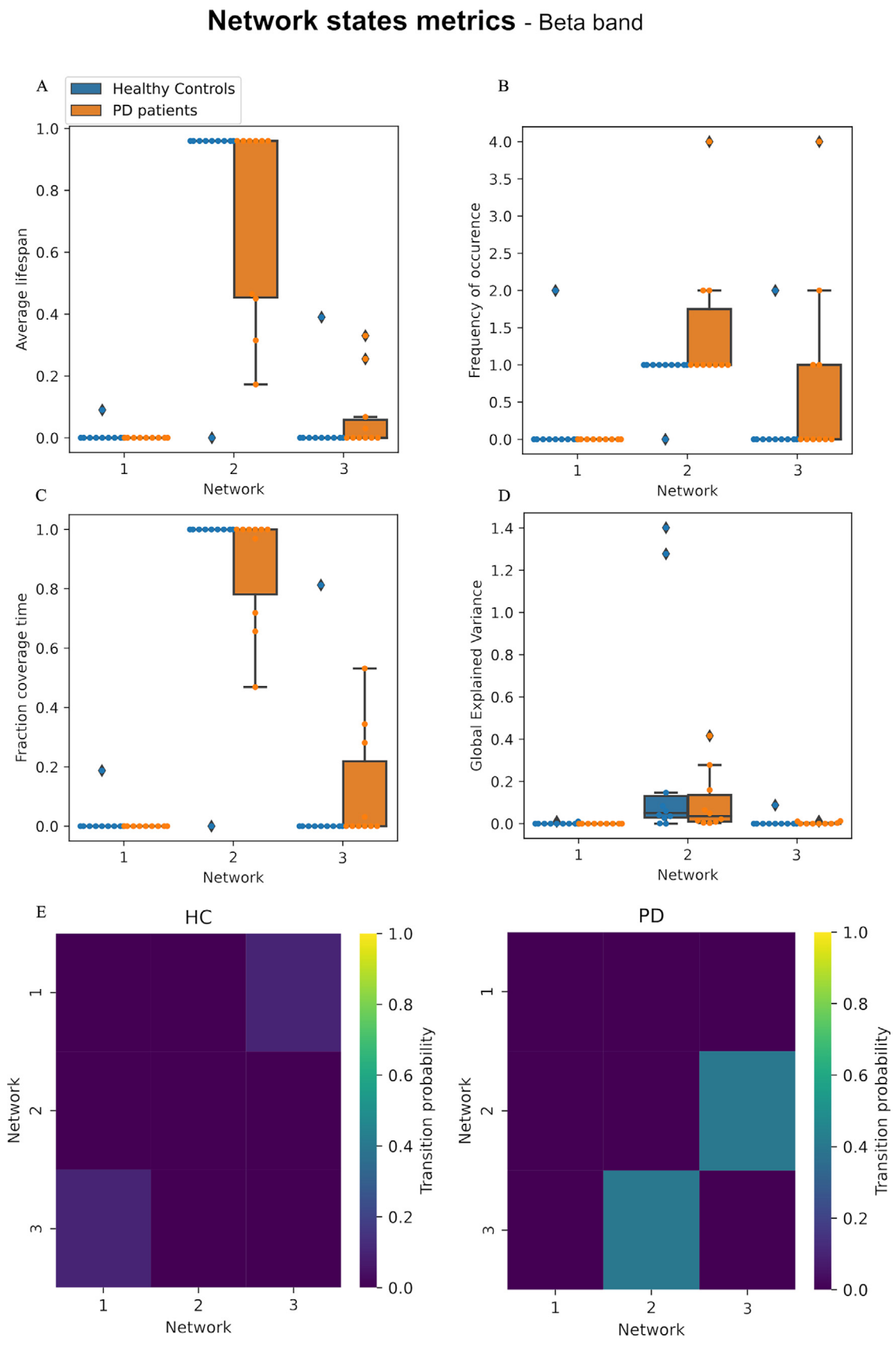



**Fig. 7.** Network states parameters and statistical analysis between HC and PD groups in the beta band. The average lifespan, frequency of occurrence, fraction coverage time, and global explained variance results are represented by colored boxplots (blue for HC group and orange for PD group) in A, B, C, and D. The transition probabilities between all dBNS are also shown in E. (For interpretation of the references to color in this figure legend, the reader is referred to the web version of this article.)

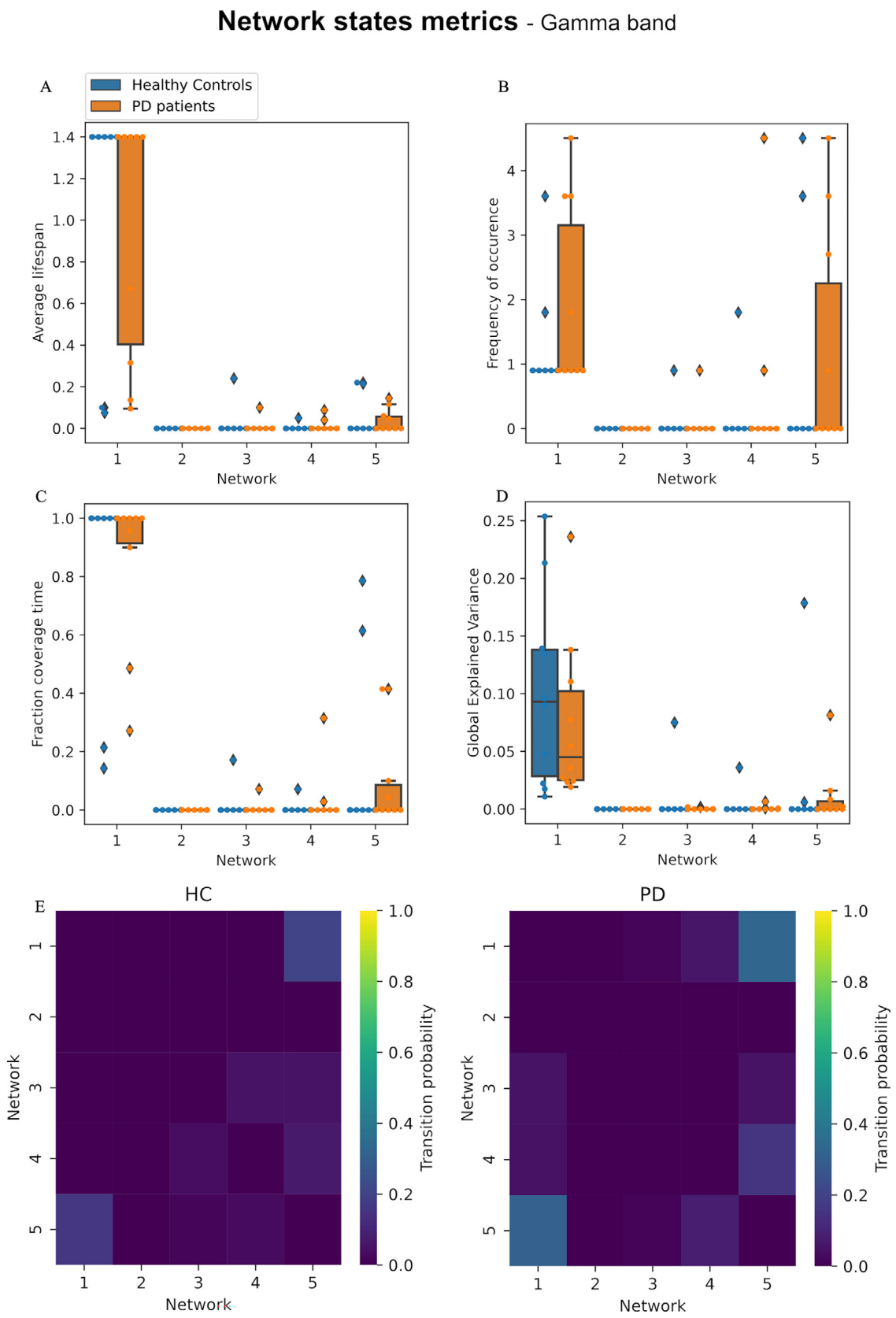



**Fig. 8.** Network states parameters and statistical analysis between HC and PD groups in the gamma band. The average lifespan, frequency of occurrence, fraction coverage time, and global explained variance results are represented by colored boxplots (blue for HC group and orange for PD group) in A, B, C, and D. The transition probabilities between all dBNS are also shown in E. (For interpretation of the references to color in this figure legend, the reader is referred to the web version of this article.)

wMNE with PLV (estimated through a sliding window approach) to track the dynamics of FC networks. To summarize dFC into a set of relevant connectivity patterns and to characterize their dynamics, a variant of temporal independent component analysis (tICA) was applied, providing a set of group-specific dynamic brain network (dBNS) states. The time-varying alterations in these states at the subject level were investigated using network states metrics. In both frequency bands (beta and gamma), dBNS with specific spatial and temporal characteristics were modulated by the task. However, microstate metrics analysis revealed no differences between PD patients and HC.

### 4.1. PD is associated with changes in cognitive action control

Among the various cognitive changes that have been associated with PD, cognitive action control (CAC) alterations are robustly reported. Some studies reported an increased global congruence effect (Praamstra et al., 1999, 1998; Schmiedt-Fehr et al., 2007; Wylie et al., 2005), others, which investigated the temporality of CAC, found changes in the dynamic expression of the process regarding impulsive action selection (Duprez et al., 2017; Wylie et al., 2009a) or suppression (van Wouwe et al., 2014; Wylie et al., 2010, 2009a, 2009b). In the present study, we found a diminished strength of impulsive action suppression in PD patients as compared to HC. Thus, our results are in line with the established description of CAC alterations in PD. It is important to note that we interpret the results according to the activation-suppression model (Ridderinkhof, 2002), and that other accounts of dynamic changes in accuracy and congruence effect have been proposed (for review, see Cespón et al., 2020). It is also worth noting that PD patients were not significantly slower than HC. However, this is probably due to the limited sample size and strong variability in RT.

### 4.2. CAC is associated with several dynamically rearranging functional networks

There has been a growing interest in the concept of functional brain states, which are characterized by a limited number of functional patterns with a temporarily stable activity followed by a fast transition to another state (Baker et al., 2014; Khanna et al., 2015; Michel and Koenig, 2018; O'Neill et al., 2018). Investigating functional brain states and their dynamic rearrangement implies the use of dimensionality reduction methods. Although K-means clustering has been commonly used in most aforementioned studies, other clustering/decomposition algorithms can also be applied to estimate dynamic brain states. Among these methods, we focused on temporal Independent Component Analysis (tICA), since it has proven its ability to track fast temporal variations in brain connectivity (O'Neill et al., 2017; Tabbal et al., 2021; Yaesoubi et al., 2015). tICA has also been applied for clinical purposes to characterize the spatiotemporal alterations induced in several brain disorders, as in Alzheimer's Disease (Koelewijn et al., 2017), epilepsy (Koelewijn et al., 2015), and depression (Knyazev et al., 2016; Nugent et al., 2015) using EEG/MEG data during rest and task. Since CAC is a dynamic process, this approach could contribute to characterizing the functional networks associated and the PD-related alterations of CAC.

Our results show that CAC can be globally described by three dominant beta networks: (i) a first one that was right-sided and mostly involved superior and inferior temporal regions, as well as cingulate and insular cortex, and inferior occipital areas; (ii) a second one that was mostly frontal; and (iii) a third one with interhemispheric fronto-temporal connections. Since we used a network-based approach, and because of the relatively high number of areas (nodes) involved in these networks, it is challenging to envision a localizationist interpretation of those results. Nevertheless, it is worth noting that these networks involve areas commonly associated with conflict resolution and inhibition found using fMRI, such as the inferior frontal gyrus, the anterior cingulate cortex, as well as orbitofrontal cortex (Aron et al., 2004; Eagle et al., 2008; Forstmann et al., 2008; Forstmann et al., 2008; Widge et al., 2019; Yeung et al., 2007). Furthermore, prefrontal beta activity has been associated with cognitive control and attention (Friedman and Robbins, 2021; Schmidt et al., 2019; Swann et al., 2009 ; for review, see Engel and Fries, 2010; Wang, 2010). In addition, these beta networks also involved temporal regions, including the fusiform area, which has been recently shown to be modulated by attentional demand in both humans and macaques (Kim et al., 2012; Sani et al., 2021; Wittfoth et al., 2006).

In addition to the nodes involved in this network, one could wonder about the general role of beta oscillations in such networks. In that respect, our results could be explained by a stimulus-induced desynchronization effect, followed by a beta rebound during the decision-making (as considered in event-related (de)synchronization studies) or as a spontaneous effect of the inhibition/activation process related to the conflict task (Panagiotaropoulos et al., 2013; Wu et al., 2019). This interpretation could be applied to the fronto-temporal network that we identified, which involved areas previously associated with decision making. However, data regarding the temporo-cingulate network showed that increased synchronization occured after the correct response, which excludes a decision-making interpretation. Another interesting account was proposed by Engel and Fries with the "Status Quo" hypothesis (Engel and Fries, 2010), which proposed that beta activity would be involved in sustaining a cognitive set when dealing with a task requiring a strong top-down component. The overall role of beta oscillations in top-down information propagation has also been supported in recent work (Miller et al., 2018). This hypothesis could also be applied to the fronto-temporal network. Indeed, the period between incongruent stimulus onset and the correct response requires a strong top-down component. In light of Engel and Fries' hypothesis and according to the role of beta oscillations in top-down processing, one would expect beta synchronization to be stronger in this period. However, this hypothesis is hard to reconcile with the temporo-cingulate network, given that it had decreased connectivity before the correct response, and increased connectivity after. That being said, cortical beta oscillations unlikely have a monolithic role, let alone in a task such as the Simon task. Indeed, the Simon task measures CAC, which in itself involves several other overlapping cognitive processes such as attention and working memory, or inhibition, and which involve strong response monitoring mechanisms. In that respect, beta oscillations were also associated with several other roles, such as activation of a cognitive set (Spitzer and Haegens, 2017), time estimation (Kulashekhar et al., 2016), default state of working memory (Lundqvist et al., 2016), or a clear-out of working memory after completion of a trial (Schmidt et al., 2019).

Regarding the gamma band, we found five significant, spatially distinct dBNS. The temporal organization of presence of these networks was considerably more complex than what we found in the beta band, and some of these networks overlapped during the task, thereby challenging interpretations. Overall, the most represented regions in these networks were frontal. Long-range connections were found within a mostly fronto-temporal network, a network with fronto-occipital connections, and networks that were mostly fronto-cingular/insular. These networks included CAC-related frontal areas, including inferior frontal, anterior cingulate and orbitofrontal regions. It is interesting to note that the prefrontal-temporal network that included most CAC-related regions in the gamma band was spatially identical to the prefrontal-temporal one in the beta band.

Similarly to beta oscillations, gamma oscillations have been associated with several cognitive functions (see (Herrmann et al., 2010) for a review). Unfortunately, studies reporting gamma effects on cognitive action control are scarce. However, some found increased gamma activity in a multi-source interference task in somato-sensory and occipital regions (Wiesman et al., 2020; Wiesman and Wilson, 2020). Among the various roles attributed to gamma oscillations, binding has probably been the most discussed. The binding theory hypothesizes that different stimulus features (color, spatial location, shape, etc.) are ultimately

binded into a single representation by the means of gamma synchronization (Engel et al., 2001; Singer, 1999). Synchronization would then be necessary for attention, sensori-motor integration and response selection. In that respect, long-range gamma connectivity, as we observed in our various brain network states, would reflect the binding of sensory and cognitive information used to perform the task. It is also possible to interpret these networks as a means of propagation of bottom-up sensory information (Miller et al., 2018). Assigning a cognitive role to gamma oscillations is nonetheless debated, and some researchers argue that gamma activity (and long-range gamma synchrony) do not necessarily have a functional role in cognition, but rather reflect local states of activation (Merker, 2016; Ray and Maunsell, 2015). Regarding PD effect on gamma oscillations, motor and frontal gamma typically show coherent activity with subcortical structures (such as the subthalamic nucleus) and might modulate the vigor of a motor response (Oswal et al., 2013). However, the gamma activity usually described in PD studies spans higher and larger gamma bands (60-90 Hz) than the one we used here (30-45 Hz). Also, although we found prefrontal gamma in our brain network states, no motor nodes were present.

### 4.3. Network presence did not differ between PD and HC at the subject-level

The use of typical microstate metrics allowed us to investigate the presence of all dBNS at the subject-level. Several metrics were used that inform on the lifespan, frequency of occurrence, coverage time, and explained variance of dBNS, as well as transition probability between states. An important point to bear in mind is that the computation of these metrics is based on the similarity between the dFC matrices of a subject, and the dBNS. At each time, one dBNS is deemed the most similar to the dFC matrix based on a spatial correlation: the dBNS with the highest correlation is considered the most similar. Consequently, for all dFC matrices, only one dBNS is set to be the most similar, although other dBNS can be present. This explains why some dBNS significantly present at the group-level had 0 values at the subject-level for the network states metrics.

Contrary to our hypothesis, we found no differences between PD patients and HC, whether examining dBNS microstates metrics in the beta or the gamma band. This absence of difference is probably explained by the fact that patients were younger and had a less severe disease than in previous behavioral studies (Cagigas et al., 2007; Duprez et al., 2017; Falkenstein et al., 2006; Wylie et al., 2010, 2005). Furthermore, the behavioral effects of PD were limited to the decrease in late inhibition as evidenced by the last slope of the delta plots, which was not associated with any microstates metrics. The only significant correlation that we found was between the first beta dBNS global explained variance and fast response accuracy, which would be hazardous to interpret since all other metrics of that dBNS were not correlated with behavior. It is also important to keep in mind that the sample size in this study is limited, thus preventing a generalizable conclusion. However, the present data nonetheless suggest that, in the case of subtle behavioral changes, there are no detectable associated differences in dynamic functional brain networks.

### 4.4. Methodological considerations and limitations

First, we focused our EEG analyses on correct incongruent trials only. At the behavioral level, CAC effects are traditionally obtained by contrasting the congruent and incongruent situations. Regarding dynamic functional brain states, it is not possible to simply subtract signals between congruent and incongruent trials to obtain networks that reflect this behavioral difference. We chose to focus on correct incongruent trials, since they reflect the implementation of CAC in the situation of highest conflict during the task. Our interpretations are thus limited to CAC in the incongruent situation, and do not reflect the traditional congruence effect observed in the behavioral data.

In this study, we used source-reconstruction methods to be able to take into account, at least partly, spatial leakage due to volume conduction, and also to make inferences at the cortical level. It is important to note that the head model used for source reconstruction was based on a standard anatomy (ICBM template) and that individual anatomy, which unfortunately was not available, would be more suited. Indeed, although it has been shown that template-based source reconstruction is reliable and yielded consistent functional networks when compared to individual anatomy (Douw et al., 2018), subject-specific changes in anatomy might impact the centroid positions of the cortical atlas which defined the nodes of our networks. Another point of caution is that source reconstruction does not completely remove all possible leakage, and the FC measure used here (PLV), is known to be sensitive to leakage. However, we chose to use this measure in order to keep true zero-lag connectivity (Finger et al., 2016; Viriyopase et al., 2012) in our data, therefore potential spurious connections might have persisted in the identified networks.

Our estimation of dynamic brain network states depended on several parameters that can be discussed, and must be kept in mind for interpreting the results.

For instance, the choice of the number of cycles and size of window overlap to compute dynamic FC is arbitrary, although we followed the recommendation of 6 cycles described in (Lachaux et al., 2000). Control analyses showed that, for the same number of cycles, changing the percentage of overlap between windows did not affect the results (see SF1). However, changing the number of cycles did. As a consequence, it has to be kept in mind that such FC results are, at least to some degree, dependent on the number of cycles.

Another important consideration is the determination of the optimal number of derived components, which is still a challenging question for most decomposition algorithms, including tICA. In this study, the selection of the number of states was performed in two consecutive steps: (1) a primary number of components was selected using the difference in data fitting (DIFFIT) technique adopted by previous studies (Timmerman and Kiers, 2000; Wang et al., 2018). Then, (2) given that all brain states are not necessarily associated with the task, we searched for components that were significantly modulated by the task. We used permutation testing by building a non-parametric null distribution generated using a 'sign-flipping' approach (Hunt et al., 2012; O'Neill et al., 2017; Winkler et al., 2014). This approach highlighted the components with trial-averaged time courses that exceeded a specific threshold. The use of the null distribution may be deemed as too conservative, since a Bonferroni correction for multiple comparisons was carried out. For example, we obtained only three significant components out of six calculated by tICA in the beta band. It could be argued that such a restrictive number of components might miss additional information. However, we did not have any *a priori* hypothesis on the number of brain states in PD or HC, nor on their duration. Therefore, a conservative approach appeared more appropriate.

We used a backfitting approach to estimate typical microstate metrics for subject-level analyses. Although this method is practical to estimate the presence of brain states at the subject-level, it suffers from a drawback which consists in assuming that only one global functional state occurs at a given moment in time. Thus, estimation of these metrics is based on the determination of one dominant dBNS at each time. This completely ignores the assumption of temporal ICA, which considers overlapping and independent brain network states with proportional weights to summarize brain activity. As a consequence, our interpretations of subject-level analyses are limited by the fact that we focused on dominant dBNS. Future studies could explore further other back-fitting approaches that rely on the notion of proportional, rather than binary, fitting.

To estimate the spatial similarity between the dBNS and dFC matrices, we used a simple correlation measure at the back-fitting step. We chose this measure since we aimed to assign to each functional network the nearest (spatially) dBNS, rather than evaluating the precision of

the exact similarity value by itself. Nevertheless, other spatial similarity metrics could be used in this context, such as those taking into account the spatial locations of the compared networks nodes (Mheich et al., 2018; Pineda-Pardo et al., 2015), or distance-based metrics (Cao et al., 2013; Gao et al., 2010).

Following the two previous considerations, an interesting point raised by our results is that the task-modulated networks that were significant for the longest periods were never the dominant networks at the subject-level. Rather, the dominant networks in both groups were always the networks with short-lived significant task modulation. This finding is puzzling, and a definitive interpretation is hard to reach without further investigation. However, we can propose a signal-to-noise ratio interpretation of that aspect. Indeed, long-lived task-modulated networks might have been found because of the group-level analysis based on the concatenation of all the dFC matrices of all trials and all subjects. tICA would be particularly efficient at finding these networks given the amount of data. At the subject-level, these networks might be too subtly present and are dominated by other networks that are less task-related, at least less specifically to the appearance of stimulus eliciting conflict. A possible way to investigate this would be to focus on prestimulus activity or on resting-state activity. In any case, this suggests that the tICA method presented in this paper is useful and robust for group-level analysis of task-related networks, but also that the use of microstates metrics might not be ideal in that context to isolate these networks at the single subject-level.

Finally, it is worth noting that investigation of dynamic functional connectivity using the methods reported here drastically constrain the analyses to relatively high frequencies. Indeed, performing the same analyses in frequencies lower than beta would have been challenging, given the limited number of cycles available in the duration of the trial. This is a key point, since most CAC-related results in the literature involve theta frequencies and report increased midfrontal theta activity during conflict (Cohen, 2014). One interesting perspective would be to investigate if the dynamic presence of certain beta brain states in PD depend on fronto-central theta activity, since midfrontal theta-parietal beta cross-frequency coupling has been shown during CAC (Duprez et al., 2020) and PD appears to be associated with decreased midfrontal theta (Singh et al., 2018).

## 5. Conclusion

In this study, we reported brain functional connectivity states at the source level that were modulated by CAC during a Simon task. At the group-level, we showed that fronto-temporal, temporo-cingulate and fronto-frontal beta and gamma networks were significantly modulated by the task. We used microstates metrics to investigate the presence of these networks at the subject-level, which revealed no differences between PD patients and HC. Our results also evidenced that the dominant network at the subject-level was never the network more durably modulated by the task at the group-level. Although tICA allowed for an estimation of task-related dynamic brain states, the use of microstates metrics might not be appropriate in the evaluation of these networks at the subject-level. Nevertheless, we believe that this study highlights the relevance of task-based dynamic connectivity measures which could help in the understanding of cognitive dysfunctions observed in PD, and in other neurological diseases.

## Funding

JD was funded by the Rennes Clinical Neuroscience Institute (INCR: www.incr.fr).

## Data and code availability statement

All the codes used to perform the analyses are available at https://github.com/jduprez/EEGcog-control_dynFC_PD.

## Declaration of Competing Interest

None.

## Credit authorship contribution statement

**Joan Duprez:** Conceptualization, Methodology, Software, Data curation, Writing – original draft, Visualization, Investigation, Validation, Writing – review & editing. **Judie Tabbal:** Methodology, Software, Data curation, Writing – original draft, Visualization, Writing – review & editing. **Mahmoud Hassan:** Conceptualization, Methodology, Writing – review & editing. **Julien Modolo:** Methodology, Writing – review & editing. **Aya Kabbara:** Writing – review & editing. **Ahmad Mheich:** Writing – review & editing. **Sophie Drapier:** Writing – review & editing. **Marc Vérin:** Writing – review & editing. **Paul Sauleau:** Conceptualization, Writing – review & editing. **Fabrice Wendling:** Writing – review & editing. **Pascal Benquet:** Conceptualization, Methodology, Data curation, Investigation, Validation, Writing – review & editing. **Jean-François Houvenaghel:** Conceptualization, Methodology, Software, Data curation, Investigation, Validation, Writing – review & editing.

## Acknowledgements

The authors would like to thank all the participants who took part in this study. We also thank Dr. Adrien Bénard (MD) and Dr. Sina Potel (MD) for their help in data acquisition. We also would like to thank Bretagne Atlantique Ambition (BAA) as well as the Rennes Clinical Neuroscience Institute (INCR: www.incr.fr), and the Ille-et-Vilaine Parkinsonian Association (APIV) who funded this work.

## Supplementary materials

Supplementary material associated with this article can be found, in the online version, at doi:10.1016/j.neuroimage.2022.119331.

## References

Allen, E.A., Damaraju, E., Eichele, T., Wu, L., Calhoun, V.D., 2018. EEG signatures of dynamic functional network connectivity states. Brain Topogr. 31, 101–116. doi:10.1007/s10548-017-0546-2.

Aron, A.R., Robbins, T.W., Poldrack, R.A., 2004. Inhibition and the right inferior frontal cortex. Trends Cogn. Sci. 8, 170–177. doi:10.1016/j.tics.2004.02.010.

Baggio, H.-C., Sala-Llonch, R., Segura, B., Marti, M.-J., Valldeoriola, F., Compta, Y., Tolosa, E., Junqué, C., 2014. Functional brain networks and cognitive deficits in Parkinson's disease. Hum. Brain Mapp 35, 4620–4634. doi:10.1002/hbm.22499.

Baggio, H.-C., Segura, B., Sala-Llonch, R., Marti, M.-J., Valldeoriola, F., Compta, Y., Tolosa, E., Junqué, C., 2015. Cognitive impairment and resting-state network connectivity in Parkinson's disease. Hum. Brain Mapp. 36, 199–212. doi:10.1002/hbm.22622.

Baker, A.P., Brookes, M.J., Rezek, I.A., Smith, S.M., Behrens, T., Probert Smith, P.J., Woolrich, M., 2014. Fast transient networks in spontaneous human brain activity. eLife 3, e01867. doi:10.7554/eLife.01867.

Barton, K., 2009. MuMIn: multi-model inference. Httpr-Forge R-Proj. Orgprojectsmumin.

Bassett, D.S., Sporns, O., 2017. Network neuroscience. Nat. Neurosci. 20, 353–364. doi:10.1038/nn.4502.

Bates, D., Mächler, M., Bolker, B., Walker, S., 2015. Fitting linear mixed-effects models using lme4. J. Stat. Softw. 67, 1–48. doi:10.18637/jss.v067.i01.

Benton, A.L., Varney, N.R., Hamsher, K.deS, 1978. Visuospatial judgment: A clinical test. Arch. Neurol. 35, 364–367.

Bola, M., Sabel, B.A., 2015. Dynamic reorganization of brain functional networks during cognition. NeuroImage 114, 398–413. doi:10.1016/j.neuroimage.2015.03.057.

Bridi, J.C., Hirth, F., 2018. Mechanisms of $\alpha$-Synuclein Induced Synaptopathy in Parkinson's Disease. Front. Neurosci. 12, 80. doi:10.3389/fnins.2018.00080.

Brodbeck, V., Kuhn, A., von Wegner, F., Morzelewski, A., Tagliazucchi, E., Borisov, S., Michel, C.M., Laufs, H., 2012. EEG microstates of wakefulness and NREM sleep. NeuroImage 62, 2129–2139. doi:10.1016/j.neuroimage.2012.05.060.

Cagigas, X.E., Filoteo, J.V., Stricker, J.L., Rilling, L.M., Friedrich, F.J., 2007. Flanker compatibility effects in patients with Parkinson's disease: impact of target onset delay and trial-by-trial stimulus variation. Brain Cogn 63, 247–259. doi:10.1016/j.bandc.2006.09.002.

Cao, B., Li, Y., Yin, J., 2013. Measuring similarity between graphs based on the levenshtein distance. Appl. Math. Inf. Sci. 7, 169–175. doi:10.12785/amis/071L24.

Cardoso, J.F., Souloumiac, A., 1993. An efficient technique for the blind separation of complex sources. In: [1993 Proceedings] IEEE Signal Processing Workshop on Higher-Order Statistics. Presented at the [1993 Proceedings] IEEE Signal Processing Workshop on Higher-Order Statistics, pp. 275–279. doi:10.1109/HOST.1993.264552.

Cespón, J., Hommel, B., Korsch, M., Galashan, D., 2020. The neurocognitive underpinnings of the Simon effect: an integrative review of current research. Cogn. Affect. Behav. Neurosci. 20, 1133–1172. doi:10.3758/s13415-020-00836-y.

Cohen, M.X., 2014. A neural microcircuit for cognitive conflict detection and signaling. Trends Neurosci. 37, 480–490. doi:10.1016/j.tins.2014.06.004.

Cong, F., He, Z., Hämäläinen, J., Leppänen, P.H.T., Lyytinen, H., Cichocki, A., Ristaniemi, T., 2013. Validating rationale of group-level component analysis based on estimating number of sources in EEG through model order selection. J. Neurosci. Methods 212, 165–172. doi:10.1016/j.jneumeth.2012.09.029.

Dale, A.M., Sereno, M.I., 1993. Improved Localizadon of Cortical Activity by Combining EEG and MEG with MRI Cortical Surface Reconstruction: A Linear Approach. J. Cogn. Neurosci. 5, 162–176. doi:10.1162/jocn.1993.5.2.162.

de Pasquale, F., Della Penna, S., Sporns, O., Romani, G.L., Corbetta, M., 2016. A dynamic core network and global efficiency in the resting human brain. Cereb. Cortex 26, 4015–4033. doi:10.1093/cercor/bhv185.

Destrieux, C., Fischl, B., Dale, A., Halgren, E., 2010. Automatic parcellation of human cortical gyri and sulci using standard anatomical nomenclature. NeuroImage 53, 1–15. doi:10.1016/j.neuroimage.2010.06.010.

Douw, L., Nieboer, D., Stam, C.J., Tewarie, P., Hillebrand, A., 2018. Consistency of magnetoencephalographic functional connectivity and network reconstruction using a template versus native MRI for co-registration. Hum. Brain Mapp. 39, 104–119. doi:10.1002/hbm.23827.

Duprez, J., Gulbinaite, R., Cohen, M.X., 2020. Midfrontal theta phase coordinates behaviorally relevant brain computations during cognitive control. NeuroImage 207, 116340. doi:10.1016/j.neuroimage.2019.116340.

Duprez, J., Houvenaghel, J.-F., Argaud, S., Naudet, F., Robert, G., Drapier, D., Vérin, M., Sauleau, P., 2017. Impulsive oculomotor action selection in Parkinson's disease. Neuropsychologia 95, 250–258. doi:10.1016/j.neuropsychologia.2016.12.027.

Eagle, D.M., Baunez, C., Hutcheson, D.M., Lehmann, O., Shah, A.P., Robbins, T.W., 2008. Stop-signal reaction-time task performance: role of prefrontal cortex and subthalamic nucleus. Cereb. Cortex 18, 178–188. doi:10.1093/cercor/bhm044.

Engel, A.K., Fries, P., 2010. Beta-band oscillations–signalling the status quo? Curr. Opin. Neurobiol. 20, 156–165. doi:10.1016/j.conb.2010.02.015.

Engel, A.K., Fries, P., Singer, W., 2001. Dynamic predictions: Oscillations and synchrony in top–down processing. Nat. Rev. Neurosci. 2, 704–716. doi:10.1038/35094565.

Falkenstein, M., Willemssen, R., Hohnsbein, J., Hielscher, H., 2006. Effects of stimulus-response compatibility in Parkinson's disease: a psychophysiological analysis. J. Neural. Transm. 113, 1449–1462.

Finger, H., Bönstrup, M., Cheng, B., Messé, A., Hilgetag, C., Thomalla, G., Gerloff, C., König, P., 2016. Modeling of large-scale functional brain networks based on structural connectivity from DTI: comparison with EEG derived phase coupling networks and evaluation of alternative methods along the modeling path. PLOS Comput. Biol. 12, e1005025. doi:10.1371/journal.pcbi.1005025.

Fornito, A., Zalesky, A., Breakspear, M., 2015. The connectomics of brain disorders. Nat. Rev. Neurosci. 16, 159–172. doi:10.1038/nrn3901.

Forstmann, B., van den Wildenberg, W., Ridderinkhof, K., 2008. Neural mechanisms, temporal dynamics, and individual differences in interference control. Cogn. Neurosci. J. Of. 20, 1854–1865.

Forstmann, B.U., Jahfari, S., Scholte, H.S., Wolfensteller, U., van den Wildenberg, W.P., Ridderinkhof, K.R., 2008. Function and structure of the right inferior frontal cortex predict individual differences in response inhibition: a model-based approach. J. Neurosci. 28, 9790–9796.

Fox, J., Weisberg, S., 2019. An R Companion to Applied Regression, Third. ed. Sage, Thousand Oaks CA.

Friedman, N.P., Robbins, T.W., 2021. The role of prefrontal cortex in cognitive control and executive function. Neuropsychopharmacology 1–18. doi:10.1038/s41386-021-01132-0.

Fries, P., 2015. Rhythms for cognition: communication through coherence. Neuron 88, 220–235.

Gao, X., Xiao, B., Tao, D., Li, X., 2010. A survey of graph edit distance. Pattern Anal. Appl. 13, 113–129. doi:10.1007/s10044-008-0141-y.

Gramfort, A., Papadopoulo, T., Olivi, E., Clerc, M., 2010. OpenMEEG: opensource software for quasistatic bioelectromagnetics. Biomed. Eng. OnLine 9, 45. doi:10.1186/1475-925X-9-45.

Graves, R.E., Bezeau, S.C., Fogarty, J., Blair, R., 2004. Boston naming test short forms: a comparison of previous forms with new item response theory based forms. J. Clin. Exp. Neuropsychol. 26, 891–902.

Hämäläinen, M.S., Ilmoniemi, R.J., 1994. Interpreting magnetic fields of the brain: minimum norm estimates. Med. Biol. Eng. Comput. 32, 35–42. doi:10.1007/BF02512476.

Hassan, M., Benquet, P., Biraben, A., Berrou, C., Dufor, O., Wendling, F., 2015. Dynamic reorganization of functional brain networks during picture naming. Cortex J. Devoted Study Nerv. Syst. Behav. 73, 276–288. doi:10.1016/j.cortex.2015.08.019.

Hassan, M., Wendling, F., 2018. Electroencephalography source connectivity: aiming for high resolution of brain networks in time and space. IEEE Signal Process. Mag. 35, 81–96. doi:10.1109/MSP.2017.2777518.

Hayes, M.T., 2019. Parkinson's Disease and Parkinsonism. Am. J. Med. 132, 802–807. doi:10.1016/j.amjmed.2019.03.001.

Herrmann, C.S., Fründ, I., Lenz, D., 2010. Human gamma-band activity: a review on cognitive and behavioral correlates and network models. Neurosci. Biobehav. Rev. 34, 981–992. doi:10.1016/j.neubiorev.2009.09.001.

Hommel, B., Wiers, R.W., 2017. Towards a unitary approach to human action control. Trends Cogn. Sci. 21, 940–949. doi:10.1016/j.tics.2017.09.009.

Hughes, A.J., Ben-Shlomo, Y., Daniel, S.E., Lees, A.J., 1992. What features improve the accuracy of clinical diagnosis in Parkinson's disease: a clinicopathologic study. Neurology 42, 1142–1146.

Hunt, L.T., Kolling, N., Soltani, A., Woolrich, M.W., Rushworth, M.F.S., Behrens, T.E.J., 2012. Mechanisms underlying cortical activity during value-guided choice. Nat. Neurosci. 15, 470–476. doi:10.1038/nn.3017.

Kabbara, A., Paban, V., Hassan, M., 2021. The dynamic modular fingerprints of the human brain at rest. NeuroImage 227, 117674. doi:10.1016/j.neuroimage.2020.117674.

Khanna, A., Pascual-Leone, A., Michel, C.M., Farzan, F., 2015. Microstates in resting-state EEG: current status and future directions. Neurosci. Biobehav. Rev. 49, 105–113. doi:10.1016/j.neubiorev.2014.12.010.

Kim, C., Johnson, N.F., Gold, B.T., 2012. Common and distinct neural mechanisms of attentional switching and response conflict. Brain Res. 1469, 92–102. doi:10.1016/j.brainres.2012.06.013.

Knyazev, G.G., Savostyanov, A.N., Bocharov, A.V., Tamozhnikov, S.S., Saprigyn, A.E., 2016. Task-positive and task-negative networks and their relation to depression: EEG beamformer analysis. Behav. Brain Res. 306, 160–169. doi:10.1016/j.bbr.2016.03.033.

Koelewijn, L., Bompas, A., Tales, A., Brookes, M.J., Muthukumaraswamy, S.D., Bayer, A., Singh, K.D., 2017. Alzheimer's disease disrupts alpha and beta-band resting-state oscillatory network connectivity. Clin. Neurophysiol. 128, 2347–2357. doi:10.1016/j.clinph.2017.04.018.

Koelewijn, L., Hamandi, K., Brindley, L.M., Brookes, M.J., Routley, B.C., Muthukumaraswamy, S.D., Williams, N., Thomas, M.A., Kirby, A., te Water Naudé, J., Gibbon, F., Singh, K.D., 2015. Resting-state oscillatory dynamics in sensorimotor cortex in benign epilepsy with centro-temporal spikes and typical brain development. Hum. Brain Mapp. 36, 3935–3949. doi:10.1002/hbm.22888.

Kötter, R., Mazziotta, J., Toga, A., Evans, A., Fox, P., Lancaster, J., Zilles, K., Woods, R., Paus, T., Simpson, G., Pike, B., Holmes, C., Collins, L., Thompson, P., MacDonald, D., Iacoboni, M., Schormann, T., Amunts, K., Palomero-Gallagher, N., Geyer, S., Parsons, L., Narr, K., Kabani, N., Goualher, G.L., Boomsma, D., Cannon, T., Kawashima, R., Mazoyer, B., 2001. A probabilistic atlas and reference system for the human brain: International Consortium for Brain Mapping (ICBM). Philos. Trans. R. Soc. Lond. B. Biol. Sci. 356, 1293–1322. doi:10.1098/rstb.2001.0915.

Kulashekhar, S., Pekkola, J., Palva, J.M., Palva, S., 2016. The role of cortical beta oscillations in time estimation. Hum. Brain Mapp. 37, 3262–3281. doi:10.1002/hbm.23239.

Lachaux, J.-P., Rodriguez, E., Le Van Quyen, M., Lutz, A., Martinerie, J., Varela, F.J., 2000. Studying single-trials of phase synchronous activity in the brain. Int. J. Bifurc. Chaos 10, 2429–2439. doi:10.1142/S0218127400001560.

Lawson, R.A., Yarnall, A.J., Duncan, G.W., Breen, D.P., Khoo, T.K., Williams-Gray, C.H., Barker, R.A., Collerton, D., Taylor, J.-P., Burn, D.J., 2016. Cognitive decline and quality of life in incident Parkinson's disease: The role of attention. Parkinsonism Relat. Disord. 27, 47–53. doi:10.1016/j.parkreldis.2016.04.009.

Lehmann, D., Faber, P.L., Galderisi, S., Herrmann, W.M., Kinoshita, T., Koukkou, M., Mucci, A., Pascual-Marqui, R.D., Saito, N., Wackermann, J., Winterer, G., Koenig, T., 2005. EEG microstate duration and syntax in acute, medication-naïve, first-episode schizophrenia: a multi-center study. Psychiatry Res. Neuroimaging 138, 141–156. doi:10.1016/j.pscychresns.2004.05.007.

Lehmann, D., Ozaki, H., Pal, I., 1987. EEG alpha map series: brain micro-states by space-oriented adaptive segmentation. Electroencephalogr. Clin. Neurophysiol. 67, 271–288 https://doi.org/10.1016/0013-4694(87)90025-3.

Lin, F.-H., Witzel, T., Ahlfors, S.P., Stufflebeam, S.M., Belliveau, J.W., Hämäläinen, M.S., 2006. Assessing and improving the spatial accuracy in MEG source localization by depth-weighted minimum-norm estimates. NeuroImage 218. doi:10.1016/j.neuroimage.2005.11.054.

Lopes, R., Delmaire, C., Defebvre, L., Moonen, A.J., Duits, A.A., Hofman, P., Leentjens, A.F.G., Dujardin, K., 2017. Cognitive phenotypes in parkinson's disease differ in terms of brain-network organization and connectivity. Hum. Brain Mapp 38, 1604–1621. doi:10.1002/hbm.23474.

Lundqvist, M., Rose, J., Herman, P., Brincat, S.L., Buschman, T.J., Miller, E.K., 2016. Gamma and beta bursts underlie working memory. Neuron 90, 152–164. doi:10.1016/j.neuron.2016.02.028.

Merker, B.H., 2016. Cortical gamma oscillations: details of their genesis preclude a role in cognition. Front. Comput. Neurosci. 10, 78. doi:10.3389/fncom.2016.00078.

Mheich, A., Hassan, M., Khalil, M., Gripon, V., Dufor, O., Wendling, F., 2018. SimiNet: a novel method for quantifying brain network similarity. IEEE Trans. Pattern Anal. Mach. Intell. 40, 2238–2249. doi:10.1109/TPAMI.2017.2750160.

Michel, C.M., Koenig, T., 2018. EEG microstates as a tool for studying the temporal dynamics of whole-brain neuronal networks: a review. NeuroImage, Brain Connect. Dyn. 180, 577–593. doi:10.1016/j.neuroimage.2017.11.062.

Miller, E.K., Lundqvist, M., Bastos, A.M., 2018. Working Memory 2.0. Neuron 100, 463–475. doi:10.1016/j.neuron.2018.09.023.

Mørup, M., Hansen, L.K., 2009. Automatic relevance determination for multi-way models. J. Chemom. 23, 352–363. doi:10.1002/cem.1223.

Nasreddine, Z.S., Phillips, N.A., Bédirian, V., Charbonneau, S., Whitehead, V., Collin, I., Cummings, J.L., Chertkow, H., 2005. The montreal cognitive assessment, MoCA: a brief screening tool for mild cognitive impairment. J. Am. Geriatr. Soc. 53, 695–699. doi:10.1111/j.1532-5415.2005.53221.x.

Nugent, A.C., Robinson, S.E., Coppola, R., Furey, M.L., Zarate, C.A., 2015. Group differences in MEG-ICA derived resting state networks: application to major depressive disorder. NeuroImage 118, 1–12. doi:10.1016/j.neuroimage.2015.05.051.

O'Neill, G.C., Tewarie, P., Vidaurre, D., Liuzzi, L., Woolrich, M.W., Brookes, M.J., 2018. Dynamics of large-scale electrophysiological networks: A technical review. NeuroImage, Brain Connect. Dyn. 180, 559–576. doi:10.1016/j.neuroimage.2017.10.003.

O'Neill, G.C., Tewarie, P.K., Colclough, G.L., Gascoyne, L.E., Hunt, B.A.E., Morris, P.G., Woolrich, M.W., Brookes, M.J., 2017. Measurement of dynamic task related functional networks using MEG. NeuroImage 146, 667–678. doi:10.1016/j.neuroimage.2016.08.061.

Oswal, A., Brown, P., Litvak, V., 2013. Synchronized neural oscillations and the pathophysiology of Parkinson's disease. Curr. Opin. Neurol. 26, 662–670. doi:10.1097/WCO.0000000000000034.

Panagiotaropoulos, T., Kapoor, V., Logothetis, N., 2013. Desynchronization and rebound of beta oscillations during conscious and unconscious local neuronal processing in the macaque lateral prefrontal cortex. Front. Psychol. 4, 603. doi:10.3389/fpsyg.2013.00603.

Pineda-Pardo, J.Á., Martínez, K., Solana, A.B., Hernández-Tamames, J.A., Colom, R., Pozo, F.del, 2015. Disparate connectivity for structural and functional networks is revealed when physical location of the connected nodes is considered. Brain Topogr. 28, 187–196. doi:10.1007/s10548-014-0393-3.

Praamstra, P., Plat, E.M., Meyer, A.S., Horstink, M.W., 1999. Motor cortex activation in Parkinson's disease: dissociation of electrocortical and peripheral measures of response generation. Mov. Disord. Off. J. Mov. Disord. Soc. 14, 790–799.

Praamstra, P., Stegeman, D.F., Cools, A.R., Horstink, M.W., 1998. Reliance on external cues for movement initiation in Parkinson's disease. Evidence from movement-related potentials. Brain J. Neurol. 121, 167–177 Pt 1.

R Core Team, 2020. R: A Language and Environment for Statistical Computing. R Foundation for Statistical Computing, Vienna, Austria.

Ray, S., Maunsell, J.H.R., 2015. Do gamma oscillations play a role in cerebral cortex? Trends Cogn. Sci. 19, 78–85. doi:10.1016/j.tics.2014.12.002.

Ridderinkhof, K.R., 2002. Activation and suppression in conflict tasks: Empirical clarification through distributional analyses.

Ridderinkhof, R.K., Forstmann, B.U., Wylie, S.A., Burle, B., van den Wildenberg, W.P., 2011. Neurocognitive mechanisms of action control: resisting the call of the Sirens. Wiley Interdiscip. Rev. Cogn. Sci. 2, 174–192.

Rutledge, D.N., Jouan-Rimbaud Bouveresse, D., 2013. Independent Components Analysis with the JADE algorithm. TrAC Trends Anal. Chem. 50, 22–32. doi:10.1016/j.trac.2013.03.013.

Sani, I., Stemmann, H., Caron, B., Bullock, D., Stemmler, T., Fahle, M., Pestilli, F., Freiwald, W.A., 2021. The human endogenous attentional control network includes a ventro-temporal cortical node. Nat. Commun. 12, 360. doi:10.1038/s41467-020-20583-5.

Schmidt, R., Ruiz, M.H., Kilavik, B.E., Lundqvist, M., Starr, P.A., Aron, A.R., 2019. Beta oscillations in working memory, executive control of movement and thought, and sensorimotor function. J. Neurosci. 39, 8231–8238. doi:10.1523/JNEUROSCI.1163-19.2019.

Schmiedt-Fehr, C., Schwendemann, G., Herrmann, M., Basar-Eroglu, C., 2007. Parkinson's disease and age-related alterations in brain oscillations during a Simon task. Neuroreport 18, 277–281. doi:10.1097/WNR.0b013e32801421e3.

Simon, J.R., Rudell, A.P., 1967. Auditory SR compatibility: the effect of an irrelevant cue on information processing. J. Appl. Psychol. 51, 300.

Singer, W., 1999. Neuronal synchrony: a versatile code for the definition of relations? Neuron 24, 49–65 https://doi.org/10.1016/S0896-6273(00)80821-1.

Singh, A., Richardson, S.P., Narayanan, N., Cavanagh, J.F., 2018. Mid-frontal theta activity is diminished during cognitive control in Parkinson's disease. Neuropsychologia 117, 113–122. doi:10.1016/j.neuropsychologia.2018.05.020.

Sizemore, A.E., Bassett, D.S., 2018. Dynamic graph metrics: Tutorial, toolbox, and tale. NeuroImage, Brain Connect. Dyn. 180, 417–427. doi:10.1016/j.neuroimage.2017.06.081.

Skidmore, F., Korenkevych, D., Liu, Y., He, G., Bullmore, E., Pardalos, P.M., 2011. Connectivity brain networks based on wavelet correlation analysis in Parkinson fMRI data. Neurosci. Lett. 499, 47–51. doi:10.1016/j.neulet.2011.05.030.

Smith, A., 1982. Symbol Digit Modalities Test (SDMT). Manual (revised). West. Psychol. Serv., Los Angel.

Spitzer, B., Haegens, S., 2017. Beyond the Status Quo: A Role for Beta Oscillations in Endogenous Content (Re)Activation. eNeuro 4. ENEURO.0170-17.2017 doi:10.1523/ENEURO.0170-17.2017.

Stroop, J.R., 1935. Studies of interference in serial verbal reactions. J. Exp. Psychol. 18, 643.

Swann, N., Tandon, N., Canolty, R., Ellmore, T.M., McEvoy, L.K., Dreyer, S., DiSano, M., Aron, A.R., 2009. Intracranial EEG reveals a time- and frequency-specific role for the right inferior frontal gyrus and primary motor cortex in stopping initiated responses. J. Neurosci. 29, 12675–12685. doi:10.1523/JNEUROSCI.3359-09.2009.

Tabbal, J., Kabbara, A., Khalil, M., Benquet, P., Hassan, M., 2021. Dynamics of task-related electrophysiological networks: a benchmarking study. NeuroImage 231, 117829. doi:10.1016/j.neuroimage.2021.117829.

Tadel, F., Baillet, S., Mosher, J.C., Pantazis, D., Leahy, R.M., 2011. Brainstorm: a user-friendly application for MEG/EEG analysis. Comput. Intell. Neurosci. 879716. doi:10.1155/2011/879716.

Tewarie, P., Liuzzi, L., O'Neill, G.C., Quinn, A.J., Griffa, A., Woolrich, M.W., Stam, C.J., Hillebrand, A., Brookes, M.J., 2019. Tracking dynamic brain networks using high temporal resolution MEG measures of functional connectivity. NeuroImage 200, 38–50. doi:10.1016/j.neuroimage.2019.06.006.

Timmerman, M.E., Kiers, H.A.L., 2000. Three-mode principal components analysis: Choosing the numbers of components and sensitivity to local optima. Br. J. Math. Stat. Psychol. 53, 1–16. doi:10.1348/000711000159132.

Tomlinson, C.L., Stowe, R., Patel, S., Rick, C., Gray, R., Clarke, C.E., 2010. Systematic review of levodopa dose equivalency reporting in Parkinson's disease. Mov. Disord. Off. J. Mov. Disord. Soc. 25, 2649–2653. doi:10.1002/mds.23429.

van den Wildenberg, W.P.M., Wylie, S.A., Forstmann, B.U., Burle, B., Hasbroucq, T., Ridderinkhof, K.R., 2010. To head or to heed? Beyond the surface of selective action inhibition: a review. Front. Hum. Neurosci. 4, 222. doi:10.3389/fnhum.2010.00222.

van Wouwe, N.C., van den Wildenberg, W.P.M., Claassen, D.O., Kanoff, K., Bashore, T.R., Wylie, S.A., 2014. Speed pressure in conflict situations impedes inhibitory action control in Parkinson's disease. Biol. Psychol. 101, 44–60. doi:10.1016/j.biopsycho.2014.07.002.

Ville, D.V.D., Britz, J., Michel, C.M., 2010. EEG microstate sequences in healthy humans at rest reveal scale-free dynamics. Proc. Natl. Acad. Sci 107, 18179–18184. doi:10.1073/pnas.1007841107.

Viriyopase, A., Bojak, I., Zeitler, M., Gielen, S., 2012. When long-range zero-lag synchronization is feasible in cortical networks. Front. Comput. Neurosci. 6.

Wang, D., Zhu, Y., Ristaniemi, T., Cong, F., 2018. Extracting multi-mode ERP features using fifth-order nonnegative tensor decomposition. J. Neurosci. Methods 308, 240–247. doi:10.1016/j.jneumeth.2018.07.020.

Wang, X.-J., 2010. Neurophysiological and computational principles of cortical rhythms in cognition. Physiol. Rev. 90, 1195–1268. doi:10.1152/physrev.00035.2008.

Wechsler, D., 1981. WAIS-R Manual: Wechsler Adult Intelligence Scale-revised. Psychological Corporation.

Widge, A.S., Heilbronner, S.R., Hayden, B.Y., 2019. Prefrontal Cortex And Cognitive Control: New Insights From Human Electrophysiology. F1000Research 8. F1000 Faculty Rev-1696 doi:10.12688/f1000research.20044.1.

Wiesman, A.I., Koshy, S.M., Heinrichs-Graham, E., Wilson, T.W., 2020. Beta and gamma oscillations index cognitive interference effects across a distributed motor network. NeuroImage 213, 116747. doi:10.1016/j.neuroimage.2020.116747.

Wiesman, A.I., Wilson, T.W., 2020. Posterior alpha and gamma oscillations index divergent and superadditive effects of cognitive interference. Cereb. Cortex 30, 1931–1945. doi:10.1093/cercor/bhz214.

Winkler, A.M., Ridgway, G.R., Webster, M.A., Smith, S.M., Nichols, T.E., 2014. Permutation inference for the general linear model. NeuroImage 92, 381–397. doi:10.1016/j.neuroimage.2014.01.060.

Wittfoth, M., Buck, D., Fahle, M., Herrmann, M., 2006. Comparison of two Simon tasks: Neuronal correlates of conflict resolution based on coherent motion perception. NeuroImage 32, 921–929. doi:10.1016/j.neuroimage.2006.03.034.

Wolters, A.F., van de Weijer, S.C.F., Leentjens, A.F.G., Duits, A.A., Jacobs, H.I.L., Kuijf, M.L., 2019. Resting-state fMRI in Parkinson's disease patients with cognitive impairment: a meta-analysis. Parkinsonism Relat. Disord. 62, 16–27. doi:10.1016/j.parkreldis.2018.12.016.

Wu, H.-M., Hsiao, F.-J., Chen, R.-S., Shan, D.-E., Hsu, W.-Y., Chiang, M.-C., Lin, Y.-Y., 2019. Attenuated NoGo-related beta desynchronisation and synchronisation in Parkinson's disease revealed by magnetoencephalographic recording. Sci. Rep. 9, 7235. doi:10.1038/s41598-019-43762-x.

Wylie, S.A., Ridderinkhof, K.R., Bashore, T.R., van den Wildenberg, W.P.M., 2010. The effect of Parkinson's disease on the dynamics of on-line and proactive cognitive control during action selection. J. Cogn. Neurosci. 22, 2058–2073. doi:10.1162/jocn.2009.21326.

Wylie, S.A., Stout, J.C., Bashore, T.R., 2005. Activation of conflicting responses in Parkinson's disease: evidence for degrading and facilitating effects on response time. Neuropsychologia 43, 1033–1043. doi:10.1016/j.neuropsychologia.2004.10.008.

Wylie, S.A., van den Wildenberg, W.P.M., Ridderinkhof, K.R., Bashore, T.R., Powell, V.D., Manning, C.A., Wooten, G.F., 2009a. The effect of Parkinson's disease on interference control during action selection. Neuropsychologia 47, 145–157.

Wylie, S.A., Van Den Wildenberg, W.P.M., Ridderinkhof, K.R., Bashore, T.R., Powell, V.D., Manning, C.A., Wooten, G.F., 2009b. The effect of speed-accuracy strategy on response interference control in Parkinson's disease. Neuropsychologia 47, 1844–1853.

Yaesoubi, M., Miller, R.L., Calhoun, V.D., 2015. Mutually temporally independent connectivity patterns: a new framework to study the dynamics of brain connectivity at rest with application to explain group difference based on gender. NeuroImage 107, 85–94. doi:10.1016/j.neuroimage.2014.11.054.

Yeung, N., Bogacz, R., Holroyd, C.B., Nieuwenhuis, S., Cohen, J.D., 2007. Theta phase resetting and the error-related negativity. Psychophysiology 44, 39–49. doi:10.1111/j.1469-8986.2006.00482.x.

Zhu, Y., Liu, J., Ye, C., Mathiak, K., Astikainen, P., Ristaniemi, T., Cong, F., 2020. Discovering dynamic task-modulated functional networks with specific spectral modes using MEG. NeuroImage 218, 116924. doi:10.1016/j.neuroimage.2020.116924.